

# Assessing national exposure and impact to glacial lake outburst floods considering uncertainty under data sparsity

Huili Chen<sup>1</sup>, Qiuhua Liang<sup>1</sup>, Jiaheng Zhao<sup>2</sup>, Sudan Bikash Maharjan<sup>3</sup>

<sup>1</sup> School of Architecture, Building and Civil Engineering, Loughborough University, Loughborough LE11 3TU, UK

5 <sup>2</sup> FM Global, 117369, Singapore

<sup>3</sup> International Centre for Integrated Mountain Development (ICIMOD), Nepal

*Correspondence to:* Qiuhua Liang (Q.Liang@lboro.ac.uk)

**Abstract.** Glacial Lake Outburst Floods (GLOFs) are widely recognized as one of the most devastating natural hazards in the Himalayas, with catastrophic consequences including substantial loss of life. To effectively mitigate these risks and enhance regional resilience, it is imperative to conduct an objective and holistic assessment of GLOF hazards and their potential impacts over a large spatial scale. However, this is challenged by the limited availability of data and the inaccessibility to most of the glacial lakes in high-altitude areas. The data challenge is exacerbated when dealing with multiple lakes across an expansive spatial area. This study aims to exploit remote sensing techniques, well-established Bayesian regression models for estimating glacial lake conditions, cutting-edge flood ~~modeling-modelling~~ technology, and open data from various sources to innovate a framework for assessing the national exposure and impact of GLOFs. In the innovative framework, multi-temporal imagery is utilized with a Random Forest model to extract glacial lake water surfaces. Bayesian models, derived from previous research, are employed to estimate a plausible range of glacial lake water volumes and associated GLOF peak discharges while accounting for the uncertainty stemming from the limited size of available data and outliers within the data. A significant number of GLOF scenarios is subsequently generated based on this estimated plausible range of peak discharges. A graphics processing unit (GPU)-based hydrodynamic model is then adopted to simulate the resulting flood hydrodynamics in different GLOF scenarios. Necessary socio-economic information is collected and processed from multiple sources, including OpenStreetMap, Google Earth, local archives, and global data products, to support exposure analysis. Established depth-damage curves are used to assess the GLOF damage extents to different exposures. The evaluation framework is applied to 21 glacial lakes identified as potentially dangerous in the Nepal Himalayas. The results indicate that [Tsho Rolpa Lake, Thulagi Lake, and Lower Barun Lake](#) bear the most serious impacts of GLOFs on buildings ~~and~~, roads and agriculture areas, while [Thulagi Lake](#) could influence existing hydropower facilities. Six anonymous lakes (located at 85°37'51" E, 28°09'44" N; 87°44'59" E, 27°48'57" N; 86°55'41" E, 27°51'00" N; 86°51'29" E, 27°41'13" N; 86°55'01" E, 27°49'55" N; 87°56'05" N, 27°47'26" E) have the potential to impact more than 200 buildings. Moreover, anonymous lake (located at 85° 37' 51" E, 28° 09' 44" N) have the potential to inundate existing hydropower facilities, and influence existing hydropower facilities, while [Tsho Rolpa Lake, Lower Barun Lake, and Lumdung Lake](#) will experience the most impacts of GLOFs on agriculture areas. Five anonymous lakes (located at 85°37'51" E, 28°09'44" N; 87°44'59" E, 27°48'57" N; 87°56'05" N, 27°47'26" E; 86°55'41" E, 27°51'00" N; 86°51'29" E, 27°41'13" N) have the potential to impact more than 200 buildings, and the first three lakes may even submerge existing hydropower facilities.

## 1 Introduction

35 Glacial Lake Outburst Floods (GLOFs) are recognized as one of the most impactful natural hazards in the Himalayas, where these disasters have had the highest death toll worldwide and caused serious economic damage (Veh et al., 2020). GLOFs can generate transient discharges that are orders of magnitude greater than the typical annual floods in the receiving rivers (Cenderelli and Wohl, 2001) and some of them can travel >200 km downstream (Richardson & Reynolds, 2000). The extreme

discharges, accelerating along the steep mountainous terrains, make GLOFs extremely destructive to downstream communities and infrastructure systems. The unpredictable nature of GLOFs, often occurring without warning, has left downstream communities and infrastructure ill-prepared, causing the loss of human lives and economic damages. The ongoing impact of climate change has introduced additional uncertainty into GLOF risk. The Himalaya region is observing extensive glacier shrinkage and a proliferation of glacial lakes (Zhang et al., 2015). The potential impacts of GLOFs on downstream communities are expected to intensify further due to population growth and socio-economic development. Hence, it is crucial to develop effective strategies for managing GLOF risks to enhance human safety and support sustainable development. This necessitates the requirement for reproducible assessment of GLOF hazards and their potential impacts arising from these glacial lakes.

Some potentially dangerous lakes have been well-studied individually, such as Tsho Rolpa Lake (e.g., Shrestha & Nakagawa, 2014), Imja Tsho Lake (e.g., Somos-Valenzuela et al., 2015), and Lower Barun Lake (e.g., Sattar et al., 2021). However, these studies provide limited insight into the overall danger and potential impacts of glacial lakes as a whole. While there have been assessments of glacial lake hazards in the Himalayan region, certain limitations exist. Previous work by Mool et al. (2011) and Bajracharya et al. (2020) employed remote sensing techniques to identify potentially dangerous glacial lakes (PDGLs) in Nepal, considering different hazard factors. Rounce et al. (2017) undertook a similar study, quantifying the hazard level of 131 glacial lakes with > 0.1 km<sup>2</sup> area in Nepal. Furthermore, Rounce et al. (2017) evaluated the potential downstream impacts of GLOFs caused by these glacial lakes using a simple flood model without any physical basis. This simple flood model has also been applied to evaluate the overall impacts of GLOFs originating from multiple glacial lakes in the Indian Himalayas (Dubey & Goyal, 2020). Zheng et al. (2021) extended their analysis to assess the impacts of GLOFs across the Third Pole by using a Geographic Information System (GIS)-based hydrological model. However, the complexity of GLOFs renders simple flood models inadequate for capturing their dynamics, thereby making them incapable of supporting detailed assessments of potential impacts on downstream communities and infrastructure.

A range of physically based hydrodynamic models ~~have~~ ~~has~~ been developed and applied to predict the spatial-temporal process of GLOFs, offering detailed insights into the resulting flood impacts (e.g., Worni et al., 2014; Ancey et al., 2019; Sattar et al., 2019). Recently, researchers have explored the use of a hydrodynamic model to assess GLOF downstream impacts in the Third Pole (Zhang et al., 2023b). However, hydrodynamic models entail a huge amount of computation and face substantial demands for computation resources when applied at a large scale. What's even more challenging is that the computational requirements increase significantly when addressing GLOF simulations involving a large number of scenarios, which is necessary for assessing GLOF's potential impact due to the complexity and uncertainty of the glacier lake breach process. Moreover, the application of hydrodynamic models to support GLOF ~~modeling~~ ~~modelling~~ and impact assessment necessitates a considerable amount of data, and data availability poses another significant challenge.

The high-alpine conditions have constrained our ability to acquire detailed spatial data for multiple lakes across a large scale. To correctly depict the dynamic inundation process of GLOFs, glacial lake conditions and dam breaching process are essential to estimating the outflow discharge resulting from a breach. While the distribution and changes of glacial lakes have been extensively mapped from increasingly available satellite imagery (e.g., Zhang et al., 2015; Nie et al., 2017; Shugar et al., 2020), accurately determining lake volume and reliably predicting dam breaching processes has remained a challenge because high-alpine conditions impede detailed fieldwork. Combining satellite imagery with existing lake bathymetry measurements offers the possibility of estimating water volumes and peak discharges from outbursts by establishing empirical relationships (e.g., Zhang et al., 2023a). However, estimated lake volumes and potential peak discharges derived from these empirical relationships can vary by up to an order of magnitude (Cook and Quincey, 2015; Muñoz et al., 2020). To account for the uncertainties inherent in conventional empirical relationships, Veh et al. (2020) developed a Bayesian robust regression, utilizing data from the bathymetric survey of 24 glacial lakes. This model estimates water volume based on the surface areas of glacial lakes. Simultaneously, they created a Bayesian variant of a physical dam-break model originally proposed by Walder

& O'Connor (1997) to predict peak discharge associated with the estimated flood volume. The Bayesian estimates explore the parameter space of plausible flood volumes and associated peak discharges, generating a million possible outburst scenarios for each lake. These scenarios comprehensively consider all potential conditions of the dam breach process for each specific lake and provide a full range of input information for hydrodynamic models, thereby facilitating predictions of the GLOF inundation process. Therefore, this study aims to leverage these established Bayesian models to support GLOF inundation simulations.

GLOF exposure and impact assessment are also restricted by data sparsity. Previous studies have typically relied on census data at coarse spatial resolutions or aggregated land use data that encompasses various objects like properties and infrastructure, to estimate the potential socio-economic impact of GLOFs (e.g., Shrestha & Nakagawa, 2014; Rounce et al., 2016). Benefiting from the emergence of new data technologies and the resulting enhancements in data quantity and quality, a spatially explicit assessment method has been developed to identify GLOF exposure at an object level and applied to the Tsho Rolpa Lake (Chen et al., 2022). Employing a similar strategy, essential socio-economic information is collected and processed from various sources, including OpenStreetMap (OSM), Google Earth, global data products, and local archives. The information is used to create a spatial exposure dataset that specifies the locations of different objects, such as individual buildings and hydropower facilities. Subsequently, this spatial exposure data is overlaid with the spatially distributed flood simulation outputs to identify potential exposure to GLOFs along their path.

Overall, this study aims to innovate a framework for object-based exposure and potential impact assessments of GLOFs for multiple lakes across a large scale by exploring the use of remote sensing techniques, the developed Bayesian regression models for estimating lake volumes and potential peak discharges, a physically based hydrodynamic model supported by parallelized high-performance computing, and socio-economic information from multiple sources. Nepal has been chosen as the test area due to its abundance of glacial lakes, and it has been reported to experience the most significant national-level economic consequences from GLOFs globally (Carrivick & Tweed, 2016).

## 2 Methodology and data

The proposed framework for object-based exposure and impact assessment of GLOFs across multiple lakes comprises several key components: extraction of glacial lake water surfaces from multi-temporal imagery, estimation of lake volumes and peak discharges using well-established Bayesian regression models, utilization of a high-performance hydrodynamic flood model accelerated by graphics processing unit (GPU) technology, and the creation of an exposure dataset sourced from open-source data (Fig. 1). In particular, leveraging multi-temporal imagery availability, a Random Forest model is developed using a set of predictor variables to delineate the maximum extent of glacial lake water surfaces. The plausible range of glacial lake water depths, volumes, and GLOF-induced peak discharges is estimated through existing Bayesian models. A substantial number of GLOF scenarios, encompassing outflow discharge hydrographs through glacial lakes, are sampled and generated based on the plausible range of peak discharges. For each scenario, the resulting outflow discharge hydrograph is employed to drive the GPU-accelerated hydrodynamic model, efficiently simulating the temporal and spatial dynamics of floods. These flood dynamics are then overlaid with the spatial exposure data to identify potential exposure to GLOFs and quantify damage extent by using established depth-damage curves.

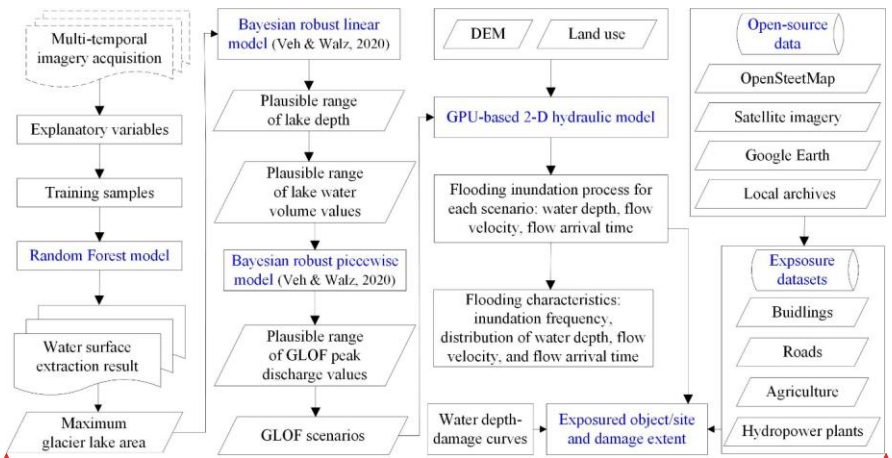


Fig. 1. GLOF exposure and impact assessment framework for multiple glacial lakes (key components highlighted in blue)

### 2.1 Glacial lake water surface extraction

With the availability of multi-temporal imagery, a Random Forest model based on a set of predictor variables is used to map the location and extent of water surfaces of glacial lakes under different hydrological conditions to produce the maximum extent of lake water surfaces.

#### 2.1.1 Acquisition of satellite imagery

Sentinel-2 is an operational multispectral imaging mission of the European Space Agency for global land observation. The Sentinel-2A and -2B satellites were launched in 2015 and 2017, respectively. These satellites capture imagery every 10 days (every 5 days with the twin satellites together). The spatial resolution for the visible and broad near-infrared (NIR) bands is 10m, while it is 20m for the red edge, narrow NIR, and short-wave infrared bands. Here, all available Sentinel-2 imagery for the case study of glacial lakes is utilized to identify the maximum extent of their water surfaces. The analysis is based on the Sentinel-2 level-1C Top-Of-Atmosphere (TOA) products, which are accessible through the Google Earth Engine. Any observations affected by clouds are masked using the Sentinel-2 Quality Assurance band flags. Bands originally at a 20-m resolution are resampled to 10m using the nearest neighbour method before being stacked for subsequent interpretation. All available Sentinel-2 datasets are collected and filtered to reserve imagery from the ablation season, reducing the impact of frozen water surfaces, as per the empirical period of the local melt season (Shugar et al., 2020). In total, 1,520 Sentinel-2 images have been collected for this purpose.

#### 2.1.2 Random Forest model

Mapping water surfaces from multiple images is a complex task that necessitates the consideration and analysis of various water-related signals in spectral responses, often influenced by water turbidity and bottom sediments. In this context, a Random Forest model is developed based on a set of predictor variables to extract water surfaces. Random Forest modeling/modelling is an ensemble classification technique (Breiman, 2001) and has been extensively used in the classification of remote sensing data (e.g., Yu et al., 2011; Rodríguez-Galiano et al., 2012). Random Forest models excel at recognizing regional variations in threshold values, surpassing the capabilities of traditional index thresholding methods (Tulbure et al., 2016). Notably, Random Forest models do not rely on data distribution assumptions and can yield accurate predictions without overfitting data.

Consequently, they have been increasingly used in water surface extraction as a ~~favorable~~ favourable alternative to traditional statistical approaches (e.g., Schaffer-Smith et al., 2017; Veh et al., 2018).

Random Forest model consists of a set of classification trees, each of which grows from a random subset of training samples and randomly permuted explanatory variables. The classification trees can grow to a specified maximum number without pruning, and the final classifications are determined by the majority votes of the trees in the forest. The explanatory variables for Sentinel-2 datasets in the Random Forest model include TOA reflectance for every spectral band, brightness temperature, vegetation indices, and water indices. TOA reflectance and brightness temperature are obtained by normalizing the target imagery, mitigating unwanted effects resulting from variations in sun angle and earth-sun distance. The vegetation indices include the Normalized Difference Vegetation Index (NDVI) and the Enhanced Vegetation Index (EVI). NDVI is sensitive to chlorophyll and used to assess terrestrial vegetation conditions (Tucker, 1979), while EVI is developed to optimize the vegetation signal in high biomass regions, de-couple canopy background signal, and reduce atmospheric influences (Huete et al., 2002). Water indices include the Normalized Difference Water Index (NDWI, McFeeters, 1996), Modified NDWI (MNDWI, Xu, 2006), and Normalized Difference Moisture Index (NDMI, Gao, 1996). NDWI enhances the response to open water features while minimizing soil and terrestrial vegetation influences. MNDWI substitutes the middle infrared band for the NIR band used in the NDWI to enhance water features and remove noise from other land types. NDMI is an effective indicator of vegetation water content. The training samples are selected via visual interpretation of satellite images to represent glacial lake water surfaces, along with various non-water covers, including diverse landscapes and vegetation types. The uncertainty in estimating glacial lake area is quantified using a widely used buffer method (Granshaw and Fountain, 2006). A buffer area of half a pixel (e.g., Zhang et al., 2015; Krause et al., 2019) is adopted to measure the uncertainty in the estimated lake area. The misclassified glacial lake water areas resulting from terrain shadows are eliminated during post-processing through manual exclusion of inaccurately classified regions.

## 2.2 GLOF dynamic inundation process simulation

Using the maximum extent of glacial lake water surfaces, we employ the established Bayesian models to predict glacial lake conditions and the dam breaching process. This allows us to estimate the full range of GLOF outflow discharge through the breach. Subsequently, various GLOF scenarios featuring a range of outflow discharge hydrographs are then sampled to drive the GPU-based hydrodynamic model for the simulation of dynamic flood dynamics resulting from GLOFs.

### 2.2.1 Estimating volumes and peak discharge of glacial lakes

Global samples from glacial lakes have suggested that the water depths for glacial lakes with similar surface areas can vary by one order of magnitude. To estimate water volumes of glacial lakes, we adopted the model that relates lake areas to their maximum depths, which was developed by Veh & Walz (2020). The model was built by compiling the reported lake areas and maximum depths obtained from bathymetric surveys conducted on 24 Himalayan glacial lakes. A Bayesian robust linear regression with a normally distributed target variable (lake depth  $d$ )  $d \sim N(\mu_d(a), 1/\tau)$  is adopted to account for possible effects of the limited sample size and outliers present in the compiled dataset. The mean  $\mu_d(a)$  is calculated below through a linear combination of the input lake area  $a$ . The precision  $\tau$  (the inverse of variance) is gamma-distributed  $\tau \sim \Gamma(0.001, 0.001)$ .

$$\mu_d(a) = \alpha_0 + \alpha_1 a \quad (1)$$

Where  $a$  is lake area, intercept  $\alpha_0 \sim N(0, 10^{-12})$ , slope  $\alpha_1 \sim N(0, 10^{-12})$ .

We obtained 100 posterior estimates for the lake depth ( $d$ ) from the Bayesian model for each lake. For each lake, samples inside the 95% highest density interval (HDI) of credible lake depth values are reserved, i.e., 94 lake depth samples for each

Formatted: Font: (Default) +Body (Times New Roman)

Formatted: Font: (Default) +Body (Times New Roman)

Formatted: Font: (Default) +Body (Times New Roman)

Formatted: Font: (Default) +Body (Times New Roman)

Formatted: Font: (Default) +Body (Times New Roman)

Formatted: Font: (Default) Cambria Math

Formatted: Font: (Default) +Body (Times New Roman)

Formatted: Font: (Default) +Body (Times New Roman)

lake. In this study, we maintained the same assumption regarding the bathymetry of the glacial lakes as outlined by Veh & Walz (2020). The delineated lake from satellite imagery is circular, and each lake is assumed to have an ellipsoidal bathymetry. Therefore, we obtained 94 estimates of total volume ( $V_{tot}$ ) for each glacial lake.

$$V_{tot} = (2/3) da \quad (2)$$

185 With regard to estimating peak discharge during dam failure, Veh & Walz (2020) built a Bayesian piecewise robust model to characterize the physically motivated model developed by Walder & O'Connor (1997). The latter model predicts peak discharge  $Q_p$  during natural dam failure. In their study, Walder & O'Connor (1997) compiled data from 63 observed natural dam breaks in various settings and identified a constant response of dimensionless peak discharge  $Qp^*$  when plotted against the dimensionless product  $\eta$  of lake volume and breach rate  $k$ . They inferred a model that describes the relationship between  
190 peak discharge and lake volume using the dimensionless peak discharge  $Qp^*$ .

$$Q_p^* = Q_p g^{-\frac{1}{2}} h^{-\frac{5}{2}} \quad (3)$$

$$\eta = V_0^* k^* \quad (4)$$

Where  $V_0^* = V_0 h^{-3}$  represents the dimensionless flood volume,  $k^* = k g^{-1/2} h^{-1/2}$  is the dimensionless breach rate,  $g$  is the acceleration of gravity,  $h$  is breach depth, and  $V_0$  is the released water volume (flood volume).  $k$  is the breach rate and subsumes lithologic conditions, the erodibility of the outflow channel, and the breach and downstream valley geometry.  $h$  is measured from the final lake surface after dam failure to the initial lake surface.  $V_0$  is the released water volume and depends on  $h$  and  $V_{tot}$ .

Empirical data support a piecewise regression model in the form  $Q_p^* = b_0 \eta^{b_1}$  ( $b_0$  and  $b_1$  are the regression parameters) for  $\eta < \eta_{c^*}$  and  $Q_p^*$  is constant for  $\eta > \eta_{c^*}$ . Bayesian piecewise linear regression was developed for predicting peak discharge  $Q_p^*$  from  $\eta$ , the product of breach rate  $k$  and released flood volume (Veh & Walz, 2020). The extent of breaching is closely linked to the geometry and material composition of the dam. To account for the most severe GLOFs, the maximum breach depth is considered up to the point where the hummocky terrain ends. To account for the most severe GLOFs, the maximum breach depth is considered to reach the marine dam's maximum depth and extend from the dam crest down to the point where the hummocky terrain ends, as determined using high-resolution satellite imagery and DEM data. The dam maximum depth data were requested from and obtained through Bajracharya et al. (2020) and are presented in Table 1. For certain lakes, the maximum breach depth can be obtained from existing studies, such as Imja Tsho Lake (Somos-Valenzuela et al., 2015), Tsho Rolpa Lake (Chen et al., 2022), Lower Barun Lake (Sattar et al., 2021), and Thulagi Lake (Maskey et al., 2020). For other lakes, the maximum breach depth was derived from high-resolution satellite imagery and terrain data available on Google Earth. The maximum breach depths for each lake are provided in Table 1. To account for the most severe GLOFs, we assume that the entire total lake volume  $V_{tot}$  would be released to create GLOFs. For each lake, we predicted the peak discharge  $Q_p$  based on a given value of  $V_{tot}$  and  $\eta$  using the Bayesian piecewise linear regression model. We generated 100 estimates of the posterior predicted  $Q_p$  for each given value of  $V_{tot}$  and  $\eta$ . The values of  $\eta$  for individual lakes encompass the assumed flood volumes, and we also considered 100 physically plausible values of the breach rate  $k$  based on a log-normal fit to reported breach rates. By multiplying the 94 samples of  $V_{tot}$  with the 100 samples of  $k$  and 100 samples of  $Q_p$ , we ultimately obtained a total of 940,000 scenarios of  $Q_p$  per lake. Considering the substantial computational resources required for GLOF inundation simulations in Section 2.2.2, 100 scenarios are selected from the 940,000  $Q_p$  and associated  $V_0$  scenarios per lake using K-means clustering. The K-means algorithm partitions the  $Q_p$  and  $V_0$  data into 100 clusters, optimizing intra-cluster homogeneity and inter-cluster heterogeneity. By selecting the data point closest to the centroid of each cluster, the selected scenarios ensure a diverse and representative sampling across the full spectrum of the dataset. 1,000 scenarios are randomly selected from the total of 940,000  $Q_p$  scenarios per lake. The weight of each selected scenario is determined by its occurrence probability,

Formatted: Font: (Default) +Body (Times New Roman)

Formatted: Font: (Default) +Body (Times New Roman)

Formatted: Font: (Default) +Body (Times New Roman)

Formatted: Font: (Default) +Body (Times New Roman)

Formatted: Font: (Default) +Body (Times New Roman)

Formatted: Font: (Default) +Body (Times New Roman)

Formatted: Font: (Default) +Body (Times New Roman)

Formatted: Font: (Default) +Body (Times New Roman)

Formatted: Font: (Default) +Body (Times New Roman)

Formatted: Font: (Default) +Body (Times New Roman)

Formatted: Font: (Default) +Body (Times New Roman)

Formatted: Font: (Default) +Body (Times New Roman)

Formatted: Font: (Default) +Body (Times New Roman)

Formatted: Font: (Default) +Body (Times New Roman)

Formatted: Font: (Default) +Body (Times New Roman)

Formatted: Font: (Default) +Body (Times New Roman)

specifically, the proportion of times its peak discharge does not exceed that of other scenarios, relative to the total number of scenarios. A smaller proportion indicates a lower likelihood of occurrence, while a larger proportion indicates a higher likelihood. The weight of each scenario is calculated by dividing the proportion by the total proportion of all possible scenarios. In these simulations, the dam breach hydrograph is assumed to have an isosceles triangle shape, simplifying its derivation from  $Q_p$  and  $V_0$ . The breach hydrograph then serves as the boundary condition for the hydrodynamic ~~modeling~~ modelling. Although there is some uncertainty, the assumption of an isosceles triangle shape for the dam breach hydrograph aligns with experimental observations (e.g., Morris et al., 2007; Walder et al., 2015; Yang et al., 2015) and is supported by simulation results from commonly used mechanisms and empirical models (e.g., Yang et al., 2023). Apart from the most severe scenarios, less severe conditions are also considered, where 25%, 50%, and 75% of the ~~maximum dam breach depth lake water volume~~ are ~~released~~reached.

### 2.2.2 2-D hydrodynamic ~~modeling~~ modelling

The High-Performance Integrated Hydrodynamic Modelling System (HiPIMS) (Zhao & Liang, 2022) is employed here to simulate the breach hydrograph. HiPIMS develops a fully dynamic model based on the 2-D depth-averaged shallow water equations. The conservative form of the governing 2-D shallow water equations is expressed as follows:

$$\frac{\partial \mathbf{q}}{\partial t} + \frac{\partial \mathbf{f}}{\partial x} + \frac{\partial \mathbf{g}}{\partial y} = \mathbf{s} \quad (5)$$

where  $t$  is the time;  $x$  and  $y$  represent the Cartesian coordinates;  $\mathbf{q}$  denotes the flow variable vector;  $\mathbf{f}$  and  $\mathbf{g}$  are the flux vectors in the  $x$ - and  $y$ -direction, respectively; and  $\mathbf{s}$  is the source term vector. The vector terms are defined as:

$$\mathbf{q} = \begin{bmatrix} h \\ q_x \\ q_y \end{bmatrix} \quad \mathbf{f} = \begin{bmatrix} q_x \\ uq_x + \frac{1}{2}gh^2 \\ uq_y \end{bmatrix}$$

$$\mathbf{g} = \begin{bmatrix} q_y \\ vq_x + \frac{1}{2}gh^2 \\ vq_y \end{bmatrix} \quad \mathbf{s} = \begin{bmatrix} 0 \\ -C_f u \sqrt{u^2 + v^2} - gh \frac{\partial z_b}{\partial x} \\ -C_f v \sqrt{u^2 + v^2} - gh \frac{\partial z_b}{\partial y} \end{bmatrix} \quad (6)$$

where  $h$  is the water depth;  $q_x = uh$  and  $q_y = vh$  are the unit-width discharges in the  $x$ - and  $y$ - directions, respectively;  $u$  and  $v$  denote the depth-averaged velocities in two Cartesian directions; and  $z_b$  is the bed elevation; and  $C_f$  is the bed roughness coefficient.

The governing equations outlined above are solved through a shock-capturing finite volume Godunov-type scheme on uniform grids (Zhao & Liang, 2022). The numerical scheme introduces a robust Godunov-type model to deliver precise and stable predictions of overland flow and flooding processes at the catchment scale. This scheme is implemented through a Python and CUDA C hybrid programming framework to achieve multi-GPU and multi-node high-performance computing for large-scale simulations. It's worth noting that the GPU-accelerated model has demonstrated computational efficiency up to ten times greater than its CPU-based counterpart (Smith & Liang, 2013). HiPIMS is set up using the terrain data and roughness data, and it is driven by the breach hydrograph for each scenario, as calculated in Section 2.2.1. Subsequently, the runoff is automatically routed throughout the flow area.

### 2.3 GLOF exposure and impact assessment

Based on the GLOF inundation process predicted by HiPIMS for each scenario, ~~which includes water depth, flow velocities, and flood arrival time,~~ we can estimate potential flood exposure by superimposing the exposure datasets onto the flood simulation results. In addition to assessing flood exposure, it is imperative to quantify the potential losses and impacts of

255 GLOFs under various conditions to understand the associated risks. Estimating the direct damage to buildings and other  
exposed objects can be achieved by employing appropriate depth-damage curves that establish the relationship between flood  
depth and the potential damage. Typically, the damage is quantified as a percentage of the cost required for repairs or  
replacements. In this study, we utilize depth-damage curves from the HAZUS Flood model to investigate the impact of GLOFs  
on buildings (Scawthorn et al., 2006). Beyond buildings, GLOFs can also have a significant impact on agricultural lands and  
260 roads. We evaluate the damage to agricultural lands and roads caused by GLOFs using the damage curves recommended in a  
technical report published by the Joint Research Centre of the European Commission (Huizinga et al., 2017). The specific  
water depth-damage curves for buildings, roads, and agricultural lands used in this study can be referenced in Chen et al.  
(2022).

#### 2.4 Data

265 HiPIMS is set up using a digital elevation model (DEM) to represent domain topography and land use data to parameterize  
domain roughness. It is driven by the out-of-breach flow discharge estimated in Section 2.2.1. The DEM used in this work is  
Shuttle Radar Topography Mission (SRTM) DEM with a spatial resolution of 30 m (Farr et al., 2007). Land use types are  
extracted from the Landsat Thematic Mapper imagery from the year 2010, provided by the International Centre for Integrated  
Mountain Development (ICIMOD, 2020). The roughness of the flow area is represented by the Manning coefficient ( $n$ ), which  
270 is dependent on land use types. The values assigned are 0.15 for forest, 0.035 for arable land, 0.03 for grassland, 0.027 for  
water surface, and 0.016 for construction land. The Manning coefficients 0.016 to 0.15 were specified based on values provided  
in earlier hydraulic textbooks or reports (such as Chow, 1959; Barnes, 1967; Arcement and Schneider, 1984), aligning with  
previous studies, for example, 0.035 to 0.17 in Nepal (Sattar et al., 2021) and 0.035 to 0.120 in Bhutan (Rinzin et al., 2023).

Open-source datasets are used to support the assessment of GLOF exposure and impacts. The OSM is a collaborative user-  
275 generated project initiated in 2004 to provide an openly available geographical database of the world, covering both the natural  
and artificial environments of the Earth's surface (OpenStreetMap contributors, 2015). While primarily built by volunteers,  
OSM also integrates geographical data contributed by governmental and specialized GIS databases for certain areas or entire  
countries, e.g., Nepal, providing relatively complete spatial data on buildings and other objects. Hydropower plant data are  
obtained from the Hydro Map project (Nepal Hydropower Portal, 2019). In the Hydro Map project, hydropower plants are  
280 categorized into three types: operation, generation, and survey. In Nepal, the hydropower licensing regime is divided into two  
stages i.e., a survey license is issued to conduct a feasibility and environmental assessment, and a generation license is granted  
after the project is found to be technically, environmentally, and economically viable. [From the Hydro Map project, Nepal  
has a total of 572 hydropower projects. These projects include 81 that are currently operational, 180 with issued generation  
licenses, and 311 with issued survey licenses.](#) Detailed information on each hydropower plant is provided, including its  
285 ~~province, district, local Government~~, capacity, commission/issue date, longitude, latitude, etc. Importing hydropower plant  
data in ArcGIS and comparing it with sub-meter imagery from ArcGIS Server and Google Earth, the positions of some  
hydropower plants are found to be inaccurate. To address the inaccuracies in the positions of some hydropower plants, a  
process has been undertaken to enhance the quality of the hydropower plant data. [Initially, we identified all hydropower  
stations located within a 2 km buffer zone along the downstream rivers of glacier lakes. For licensed hydropower plants that  
290 were not situated on the river, we relocated them to the nearest river point, ensuring they were accurately placed on the river  
as indicated by the Hydro Map project. For operational rivers, we used high-resolution remote sensing imagery from sources  
such as Google Maps and Google Earth to precisely determine their locations.](#)

~~The coordinates of existing hydropower plants, including those in operation and under construction, have been collected from  
Wikipedia. These coordinates are then visually inspected and collected against sub-meter imagery obtained from ArcGIS~~

Formatted: Font: (Default) +Body (Times New Roman)

Formatted: Font: (Default) +Body (Times New Roman)

Formatted: Font: (Default) +Body (Times New Roman)

Formatted: Font: (Default) +Body (Times New Roman)

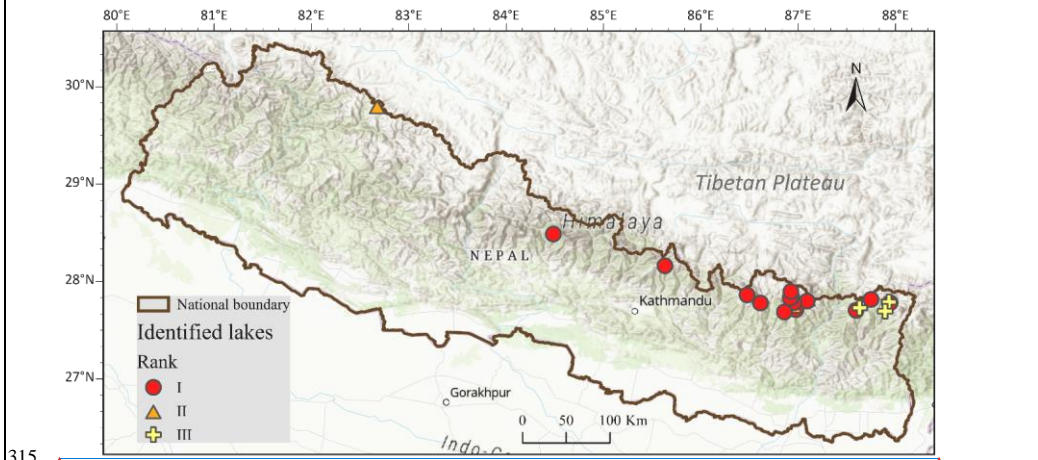


295 Server and Google Earth, as they are discernible in sub-meter imagery. The newly collected coordinates will be utilized to  
update the spatial positions of hydropower plants provided by the Hydro Map project.

### 3 Study area and glacial lakes

300 Nepal is highly vulnerable to GLOFs. A total of 53 GLOF events have been documented in Nepal from 1560 to now (Shrestha  
et al., 2023). Additionally, there have been 37 GLOF events recorded in the Tibetan Autonomous Region, China, that had  
transboundary impacts on Nepal. These historical events have had devastating consequences for the country. For example,  
both the 1985 Dig Tsho GLOF and the 1998 Tam Pokhari GLOF had devastating effects, resulting in significant loss of life,  
property and infrastructure damage, and severe disruptions to the livelihoods of those living in downstream areas.  
Approximately 1.56 million people live downstream within 3 km of moraine-dammed lakes in Nepal, putting them at risk of  
GLOFs (Ghimire, 2004). If climate change continues at its present pace, rates of glacier mass loss and shrinkage and the  
305 formation and expansion of glacial lakes will increase further, which could escalate the occurrence of GLOFs. Exacerbating  
the situation, GLOF exposure and risk are on the rise due to the expansion of settlements, economic activities, and  
infrastructure construction along riverbanks.

In Nepal, a total of 2,070 glacial lakes with lake areas equal to or larger than 0.003 km<sup>2</sup> have been identified and mapped using  
Landsat images (Bajracharya et al., 2020). These glacial lakes are predominantly situated in northern Nepal, at elevations  
310 ranging from 3400m to 5908m. Notably, 98% of these glacial lakes are positioned above 4000m. Bajracharya et al. (2020)  
assessed GLOF hazard factors related to lake and dam characteristics, glacier activity at the source, and the morphology of the  
lake surroundings for the 2,070 glacial lakes. They identified 21 lakes as PDGLs (Fig 2 and Table 1). Among the 21 PDGLs,  
some lakes have names, while others do not and were designated as 'Anonymous'. [These 21 PDGLs are further categorized](#)  
[into three ranks based on the level of danger associated with GLOF hazards, with Rank I representing the highest level of risk.](#)



Formatted: Font: (Default) +Body (Times New Roman)

Formatted: Font: (Default) +Body (Times New Roman)

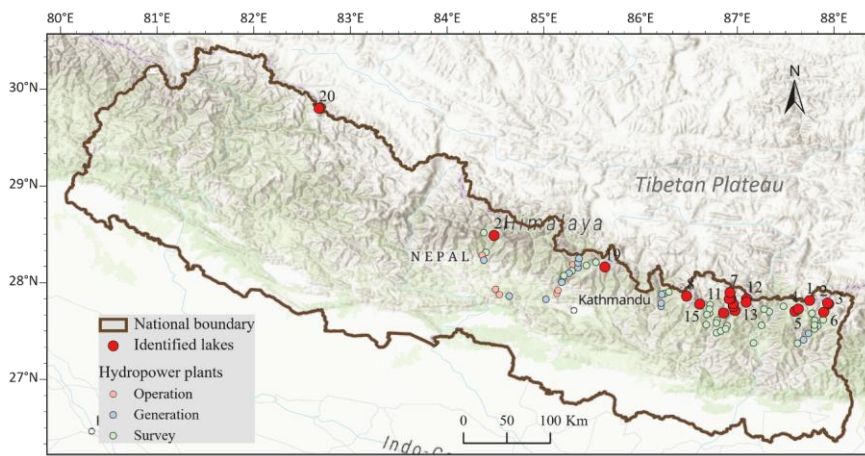


**Fig 2. Study area, and 21 identified dangerous glacial lakes each with a unique lake number, and potentially impacted hydropower plants, and their danger level rank of GLOF hazards with Rank I being the highest.**

In this study, the focus is on these 21 PDGLs, and a comprehensive assessment of their GLOF risk and downstream impacts is conducted. Each lake is assessed using the proposed evaluation framework in Section 2. The model and evaluation domain for each lake are determined based on the maximum potential inundation extent resulting from GLOFs, as well as the topographic features and river network conditions downstream. Typically, the domain spans more than 100 km and is sufficiently extensive to encompass all potential impacts.

Formatted: Font: (Default) +Body (Times New Roman)

Formatted: Font: (Default) +Body (Times New Roman), (Asian) +Body Asian (SimSun), (Asian) Chinese (Simplified, Mainland China)

Table 1 Delineated glacial lake areas under varied water-occurrence frequency from multi-temporal Sentinel-2 imagery

| Lake number | Lake ID         | Lake name    | Maximum depth of dam (m) | Longitude (E) | Latitude (N) | Area (km <sup>2</sup> ) (> 5%) | Area (km <sup>2</sup> ) (> 25%) | Area (km <sup>2</sup> ) (> 50%) |
|-------------|-----------------|--------------|--------------------------|---------------|--------------|--------------------------------|---------------------------------|---------------------------------|
| 1           | GL087749E27816N | Anonymous 1  | 221                      | 87°44'59"     | 27°48'57"    | 0.178 ± 0.011                  | 0.169 ± 0.011                   | 0.161 ± 0.011                   |
| 2           | GL087934E27790N | Anonymous 2  | 128                      | 87°56'05"     | 27°47'26"    | 0.148 ± 0.012                  | 0.134 ± 0.012                   | 0.112 ± 0.010                   |
| 3           | GL087945E27781N | Anonymous 3  | 124                      | 87°56'42"     | 27°46'51"    | 0.048 ± 0.005                  | 0.040 ± 0.005                   | 0.035 ± 0.004                   |
| 4           | GL087632E27729N | Anonymous 4  | 63                       | 87°37'55"     | 27°43'44"    | 0.036 ± 0.004                  | 0.032 ± 0.004                   | 0.016 ± 0.005                   |
| 5           | GL087596E27705N | Anonymous 5  | 158                      | 87°35'46"     | 27°42'18"    | 0.026 ± 0.003                  | 0.020 ± 0.003                   | 0.010 ± 0.003                   |
| 6           | GL087893E27694N | Anonymous 6  | 51                       | 87°53'36"     | 27°41'41"    | 0.037 ± 0.005                  | 0.028 ± 0.005                   | 0.015 ± 0.004                   |
| 7           | GL086925E27898N | Imja Tsho    | 55                       | 86°55'30"     | 27°53'53"    | 1.741 ± 0.047                  | 1.630 ± 0.042                   | 1.561 ± 0.041                   |
| 8           | GL086476E27861N | Tsho Rolpa   | 159                      | 86°28'34"     | 27°51'40"    | 1.712 ± 0.043                  | 1.657 ± 0.041                   | 1.610 ± 0.040                   |
| 9           | GL086928E27850N | Anonymous 7  | 45                       | 86°55'41"     | 27°51'00"    | 0.553 ± 0.021                  | 0.533 ± 0.021                   | 0.510 ± 0.022                   |
| 10          | GL086935E27838N | Hongu 1      | 43                       | 86°56'06"     | 27°50'17"    | 0.322 ± 0.018                  | 0.305 ± 0.018                   | 0.293 ± 0.018                   |
| 11          | GL086917E27832N | Anonymous 8  | 128                      | 86°55'01"     | 27°49'55"    | 0.361 ± 0.015                  | 0.342 ± 0.014                   | 0.332 ± 0.014                   |
| 12          | GL087095E27829N | Anonymous 9  | 61                       | 87°05'42"     | 27°49'44"    | 0.118 ± 0.008                  | 0.114 ± 0.008                   | 0.037 ± 0.012                   |
| 13          | GL087092E27798N | Lower Barun  | 128                      | 87°05'31"     | 27°47'53"    | 2.193 ± 0.048                  | 2.044 ± 0.046                   | 1.900 ± 0.053                   |
| 14          | GL086957E27783N | Hongu 2      | 382                      | 87°57'25"     | 27°46'59"    | 0.872 ± 0.030                  | 0.865 ± 0.030                   | 0.843 ± 0.030                   |
| 15          | GL086612E27779N | Lumding      | 62                       | 86°36'43"     | 27°46'44"    | 1.475 ± 0.037                  | 1.411 ± 0.034                   | 1.349 ± 0.035                   |
| 16          | GL086958E27755N | Chamlang     | 212                      | 86°57'29"     | 27°45'18"    | 0.921 ± 0.027                  | 0.856 ± 0.021                   | 0.700 ± 0.026                   |
| 17          | GL086977E27711N | Anonymous 10 | 129                      | 86°58'37"     | 27°42'40"    | 0.085 ± 0.007                  | 0.074 ± 0.007                   | 0.009 ± 0.003                   |
| 18          | GL086858E27687N | Anonymous 11 | 172                      | 86°51'29"     | 27°41'13"    | 0.336 ± 0.015                  | 0.324 ± 0.015                   | 0.307 ± 0.014                   |
| 19          | GL085630E28162N | Anonymous 12 | 223                      | 85°37'51"     | 28°09'44"    | 0.150 ± 0.009                  | 0.137 ± 0.008                   | 0.124 ± 0.008                   |
| 20          | GL082673E29802N | Anonymous 13 | 99                       | 82°40'27"     | 29°48'09"    | 0.047 ± 0.006                  | 0.041 ± 0.005                   | 0.032 ± 0.005                   |
| 21          | GL084485E28488N | Thulagi      | 192                      | 84°29'06"     | 28°29'17"    | 0.997 ± 0.032                  | 0.964 ± 0.032                   | 0.921 ± 0.029                   |

Formatted: Font: (Default) +Body (Times New Roman)

Formatted Table

Formatted: Font: (Default) +Body (Times New Roman)

Formatted: Font: (Default) +Body (Times New Roman)

Formatted: Font: (Default) +Body (Times New Roman)

Formatted: Font: (Default) +Body (Times New Roman)

Formatted: Font: (Default) +Body (Times New Roman)

Formatted: Font: (Default) +Body (Times New Roman)

Formatted: Font: (Default) +Body (Times New Roman)

Formatted: Font: (Default) +Body (Times New Roman)

Formatted: Font: (Default) +Body (Times New Roman)

Formatted: Font: (Default) +Body (Times New Roman)

Formatted: Font: (Default) +Body (Times New Roman)

Formatted: Font: (Default) +Body (Times New Roman)

Formatted: Font: (Default) +Body (Times New Roman)

Formatted: Font: (Default) +Body (Times New Roman)

Formatted: Font: (Default) +Body (Times New Roman)

Formatted: Font: (Default) +Body (Times New Roman)

Formatted: Font: (Default) +Body (Times New Roman)

Formatted: Font: (Default) +Body (Times New Roman)

Formatted: Font: (Default) +Body (Times New Roman)

Formatted: Font: (Default) +Body (Times New Roman)

Formatted: Font: (Default) +Body (Times New Roman)

Formatted: Font: (Default) +Body (Times New Roman)

325

## 4 Results

### 4.1 Glacial Lake Water Surface Extraction

Water surfaces of glacial lakes are delineated from Sentinel-2 images using the Random Forest model, as previously outlined. The Random Forest model is trained with a set of training samples that comprise both water and non-water features. To account for seasonal variations in lake water surfaces, the training samples for water features are manually selected from images acquired at different times. Various non-water features encompass diverse landscapes and vegetation types. This training dataset is subsequently employed to drive and train the Random Forest model, which is then employed to delineate water surfaces for all the adopted Sentinel-2 images. The subsequent analysis involves the computation of water-occurrence frequency based on multi-temporal water surfaces. The outcomes of water-occurrence frequency for specific representative lakes are visually presented in Fig. 3. It is noteworthy that lake areas are not consistently characterized by open water throughout the year. For instance, lake 'Anonymous 1' ( $87^{\circ} 44' 59''$  E,  $27^{\circ} 48' 57''$  N) (Fig. 3(b)) exhibits an average water-occurrence frequency of 72%, while lake 'Anonymous 2' ( $87^{\circ} 56' 05''$  E,  $27^{\circ} 47' 26''$  N) (Fig. 3(d)) has an average water-occurrence frequency of 58%. In contrast, for certain lakes, like 'Anonymous 8' ( $86^{\circ} 55' 01''$  E,  $27^{\circ} 49' 55''$  N) and the Tsho Rolpa Lake, lake areas are always covered with water. Hence, the capacity to map glacial lakes to assess the associated GLOF risk is influenced by the timing of image acquisition.

Table 1 presents the determined lake areas based on varying water-occurrence frequencies. To mitigate the effects of misinterpretations, such as cloud shadows, a 5% threshold is utilized to exclude areas characterized by low water-occurrence frequencies. Subsequently, the maximum lake boundary is delineated for each lake, allowing for the straightforward calculation of maximum lake areas. Among the 21 lakes, the largest one is Lower Barun Lake, a substantial glacial lake in Nepal known for its depth and size. Its area measures  $2.193 \pm 0.048$  km<sup>2</sup>, while the smallest lake (Anonymous 5;  $87^{\circ} 35' 46''$  E,  $27^{\circ} 42' 18''$  N) covers only  $0.026 \pm 0.003$  km<sup>2</sup>. Lower Barun Lake, along with the second largest PDGL, Imja Tsho Lake, has undergone significant area growth. The estimated maximum area of Imja Tsho Lake here is  $1.741 \pm 0.047$  km<sup>2</sup>. Tsho Rolpa Lake boasts a maximum area estimated at  $1.712 \pm 0.043$  km<sup>2</sup>. This aligns with previous findings, which reported that the lake had an area of 0.23 km<sup>2</sup> in 1957, which grew to 1.02 km<sup>2</sup> in 1979, 1.65 km<sup>2</sup> in 1999, and 1.61 km<sup>2</sup> in 2019 (Chen et al., 2021). Lumding Lake, another PDGL with an estimated area exceeding 1 km<sup>2</sup>, displayed notable growth. It had an area of 0.104 km<sup>2</sup> in 1963, 0.66 km<sup>2</sup> in 1987, 0.8 km<sup>2</sup> in 1996, and 1.18 km<sup>2</sup> in 2016 (Khadka et al., 2019). Our assessment indicates that the maximum area of Lumding Lake is  $1.475 \pm 0.037$  km<sup>2</sup>. In summary, the estimated maximum lake areas derived from multi-temporal satellite images for these extensively studied lakes are in good agreement with previous research. To establish the maximum lake boundary for potential risk assessment, it is imperative to leverage multi-temporal imagery capturing various hydrological conditions of glacial lakes.

The maximum areas of the four large lakes (Lower Barun, Imja Tsho, Tsho Rolpa, and Lumding), each exceeding 1 km<sup>2</sup>, are approximately 1.1 times the extent to which water covers more than 50% of the time. In contrast, for the comparatively smaller lakes (Anonymous 3, 4, 5, 6, 10, and 13), the ratio of maximum area to the area covered by water for more than 50% of the time can be as high as 1.4 to 2.5 times. For instance, 'Anonymous 10' ( $86^{\circ} 58' 37''$  E,  $27^{\circ} 42' 40''$  N) has a maximum area of 0.085 km<sup>2</sup>, while only 0.009 km<sup>2</sup> is covered with water for more than 50% of the time. The areas of small PDGLs exhibit more significant variations in space and time compared to those of larger PDGLs, making the associated risks more uncertain. Additionally, the ratio of maximum area to the area covered by water for more than 50% of the time is predominantly in the range of 1.1 to 1.5 for PDGLs with high hazard level I. However, for PDGLs with lower hazard levels II and III, this

ratio varies from 1.3 to 3.2. This indicates that the areas of PDGLs with a high hazard level exhibit more stability in terms of space and time compared to those with lower hazard levels.

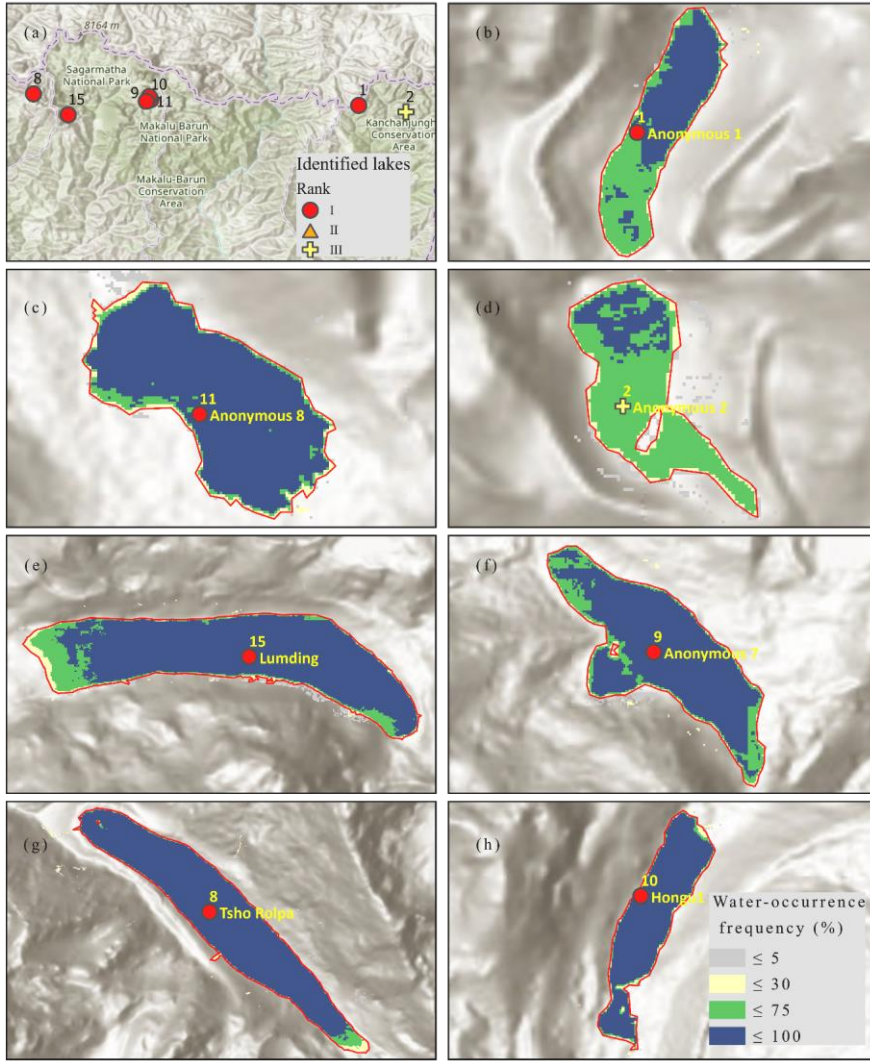


Fig 3 Water surfaces extracted from multi-temporal Sentinel-2 imagery in representative glacial lakes in Nepal (lake numbers and other lake details can be found in Table 1)

#### 4.2 Lake volumes and peak discharges prediction

We obtained 94 estimates of the total volume  $V_{tot}$  (Fig 4 (a)) and flood volume  $V_f$  (Fig 4 (b)) for each lake (Fig 4 (a)) and a total of 940,000 scenarios of peak discharge  $Q_p$  per lake (Fig 4 (cb)) using the models introduced in Section 2.2.1. The average lake volumes and peak discharges of the 21 PDGLs span more than 2 and 3 orders of magnitude. Figure 4 (a) clearly illustrates the variation in total volumes among the 21 PDGLs, with Lower Barun (Number 13) standing out as the most substantial voluminous, possessing a median value of approximately  $24208.28 \times 10^6$  million- $m^3$ . In contrast, Anonymous 5

Formatted: Font: (Default) +Body (Times New Roman)

Formatted: Font: (Default) +Body (Times New Roman)

Formatted: Font: (Default) +Body (Times New Roman)

Formatted: Font: (Default) +Body (Times New Roman), Superscript

Formatted: Font: (Default) +Body (Times New Roman)

375 (Number 5) is the smallest, with a median volume of approximately  $226.7204.0 \times 10^3$  thousand  $m^3$ . The disparity between these two lakes is striking, as Lower Barun's median volume is approximately 1000 times greater than that of Anonymous 5.

We collected geophysical investigation data for named PDGLs and compared them against calculated volumes using field-investigated lake areas, as shown in Table 2. While there are some inconsistencies, the calculated volumes generally align with the investigated values. For example, the Lower Barun glacial lake has an average estimated floodlake volume of  $238.9 \times 10^6$   $m^3$  and an average estimated peak discharge of  $18,240 m^3/s$ . The water volume of the Lower Barun glacial lake in 2015 was approximately  $112.3 \times 10^6 m^3$ , with a lake area of  $1.52 km^2$  based on bathymetric measurements. Using the established relationship between lake area and volume, the average volume for a lake with a  $1.52 km^2$  area is calculated to be  $108.27 \times 10^6 m^3$ , which closely matches the measured volume of the Lower Barun glacial lake. For the smallest lake (Anonymous 5) among these 21 PDGLs, its average volume and peak discharge are  $0.22 \times 10^6 m^3$  and  $167 m^3/s$ , respectively. This means that the average volume and peak discharge of the Lower Barun glacial lake are 1,041 and 108 times greater than those of the smallest lake, respectively.

385 Figure 4 (b) highlights the substantial variation in potential flood volumes across the lakes under the most extreme scenarios, with Lower Barun exhibiting the highest median flood volume, while Anonymous 6 (Number 6)5 has the lowest. Notably, the median flood volume of Lower Barun is approximately 21,50160 times greater than that of Anonymous 65. According to Figure 4(c) showing the distribution of peak discharges, Lower Barun has the highest median peak discharge at  $21,810.521.3 \times 10^3 m^3/s$ . Following it are Lunding, Imja Tsho and Tsho Rolpa Tsho Rolpa, Thulagi, Imja Tsho, and Lunding, which all have similar peak discharge magnitudes ranging from 513,000 to 105,000  $m^3/s$ . The lake with the lowest peak discharge is Anonymous 6, with a discharge of  $10.0154.1 m^3/s$ . The peak discharge of Lower Barun is approximately 2,000140 times greater than that of Anonymous 6.

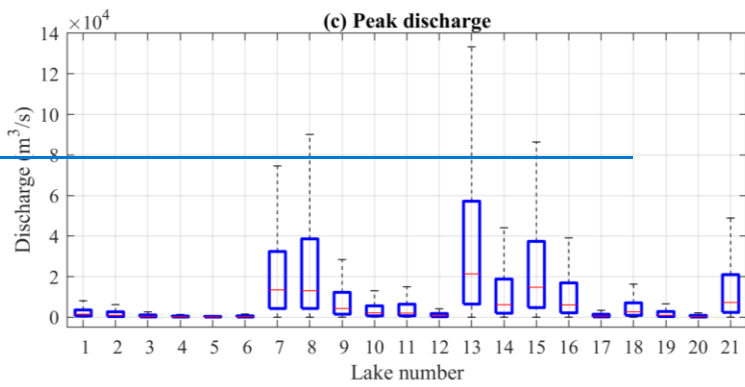
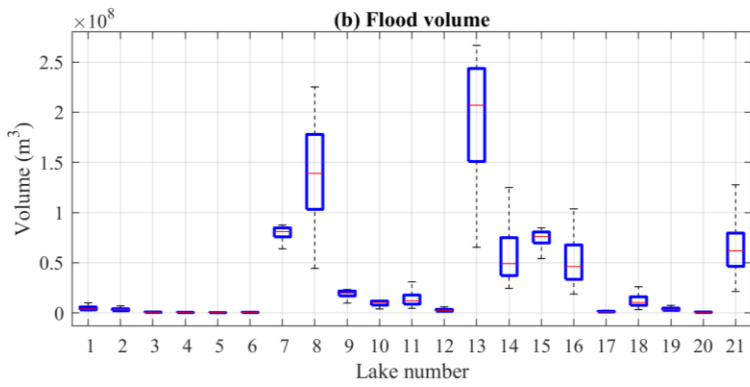
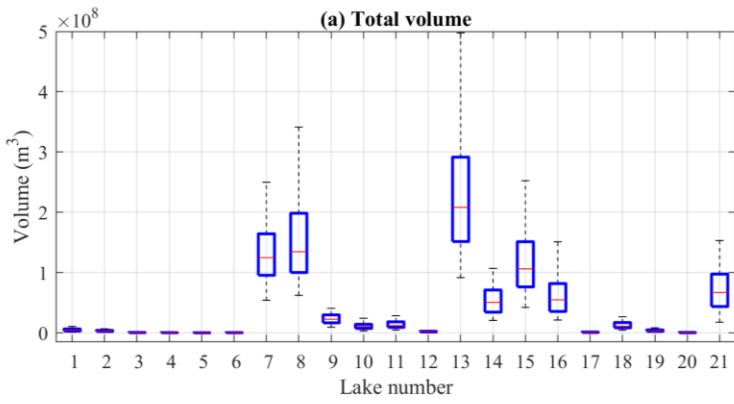
Formatted: Font: (Default) +Body (Times New Roman), Superscript

Formatted: Font: (Default) +Body (Times New Roman)



Formatted: Font: (Default) +Body (Times New Roman)

Formatted: Font: (Default) +Body (Times New Roman)



395

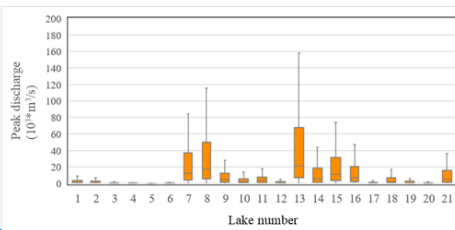
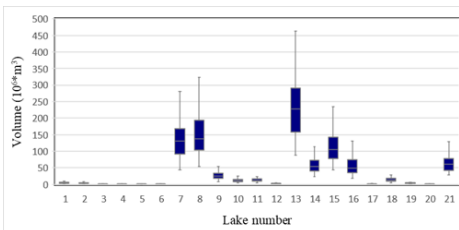


Fig 4 (a) Estimated [total volume](#), (b) [lake flood](#) volumes and (c) [estimated](#) peak discharges for each glacial lake

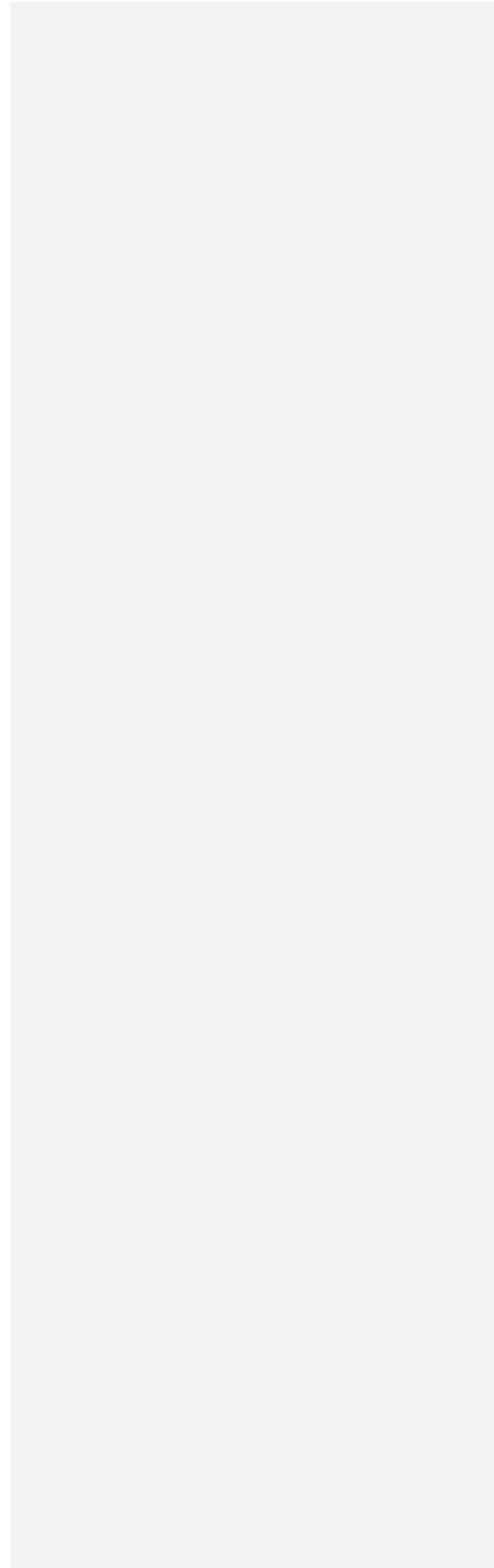




Table 2 Comparisons between the lake areas (km<sup>2</sup>) and volumes (10<sup>6</sup>m<sup>3</sup>) derived from bathymetric investigations and those calculated in this study for named lakes.

| Lake number | Lake name   | Maximum areas | Median Estimated volume        | Investigation year | Investigated areas | Investigated volume | Calculated volume for the investigated areas | Reference                 |
|-------------|-------------|---------------|--------------------------------|--------------------|--------------------|---------------------|--|---------------------------|
| 7           | Imja Tsho   | 1.741         | <del>131.16135</del><br>124.9  | 2016               | 1.35               | 88                  | 87.576                                       | Lala et al., (2017)       |
| 8           | Tsho Rolpa  | 1.712         | <del>138.39135</del><br>9134.7 | 1994               | 1.39               | 76.45               | 92.14  | Rana et al., (2000)       |
| 13          | Lower Barun | 2.193         | <del>238.86212</del><br>208.2  | 2015               | 1.52               | 112.3               | 108.273                                      | Haritashya et al., (2018) |
| 15          | Lumding     | 1.475         | <del>103.16104</del><br>7106.2 | 2015               | 1.13               | 57.7                | 65.93  | Rounce et al., (2016)     |
| 16          | Chamlang    | 0.921         | <del>49.5355.94</del><br>54.9  | 2009               | 0.87               | 34.9 - 35.6         | 45.758                                       | Lamsal et al., (2016)     |
| 21          | Thulagi     | 0.997         | <del>59.6957.34</del><br>67.1  | 2017               | 0.89               | 36                  | 47.12  | Haritashya et al., (2018) |

Formatted: Font: (Default) +Body (Times New Roman)

Formatted: Font: (Default) +Body (Times New Roman)

Formatted: Font: (Default) +Body (Times New Roman)

Formatted: Font: (Default) +Body (Times New Roman)

Formatted: Font: (Default) +Body (Times New Roman)

Formatted: Font: (Default) +Body (Times New Roman)

Formatted: Font: (Default) +Body (Times New Roman)

Formatted: Font: (Default) +Body (Times New Roman)

400 **4.3 Flood inundation simulation**

**4.3.1 Inundation areas**

HiPIMS is used to simulate flood dynamics in 1,000 scenarios for each lake with maximum dam depth breached and the lake water volume released. The final flood inundation probability and maximum water depth are derived from each scenario's results multiplied by their respective weight. Herein, we use the simulation results from Imja Tsho Lake and Lower Barun Lake as illustrative examples (Fig. 5). The areas with high flood inundation probabilities are predominantly distributed along the downstream valley. The areas with flood inundation frequency exceeding 50% can be substantial, reaching 51,295.6 km<sup>2</sup> for Imja Tsho Lake and 65,320.4 km<sup>2</sup> for Lower Barun Lake. The maximum water depth offers spatial insights into the potential severity of GLOFs in downstream areas (Fig. 5(c) and 5(d)). It facilitates the identification of areas characterized by both high inundation probability and significant maximum water depth. For instance, concerning Lower Barun Lake, there are 6,127.4 km<sup>2</sup> of areas exhibiting both inundation frequency exceeding 90% and maximum water depth exceeding 40.5 m. These specific areas should undoubtedly receive heightened attention in future flood risk management and mitigation.

Formatted: Font: (Default) +Body (Times New Roman)

Formatted: Font: (Default) +Body (Times New Roman), Font color: Text 1

Formatted: Font: (Default) +Body (Times New Roman), Font color: Red

Formatted: Font: (Default) +Body (Times New Roman)

Formatted: Font: (Default) +Body (Times New Roman), Font color: Auto

Formatted: Font: (Default) +Body (Times New Roman)

Formatted: Font: (Default) +Body (Times New Roman), Font color: Auto

Formatted: Font: (Default) +Body (Times New Roman)

Formatted: Font: (Default) +Body (Times New Roman), Font color: Auto

Formatted: Font: (Default) +Body (Times New Roman), Font color: Auto

Formatted: Font: (Default) +Body (Times New Roman)

Formatted: Font: (Default) +Body (Times New Roman), Font color: Red

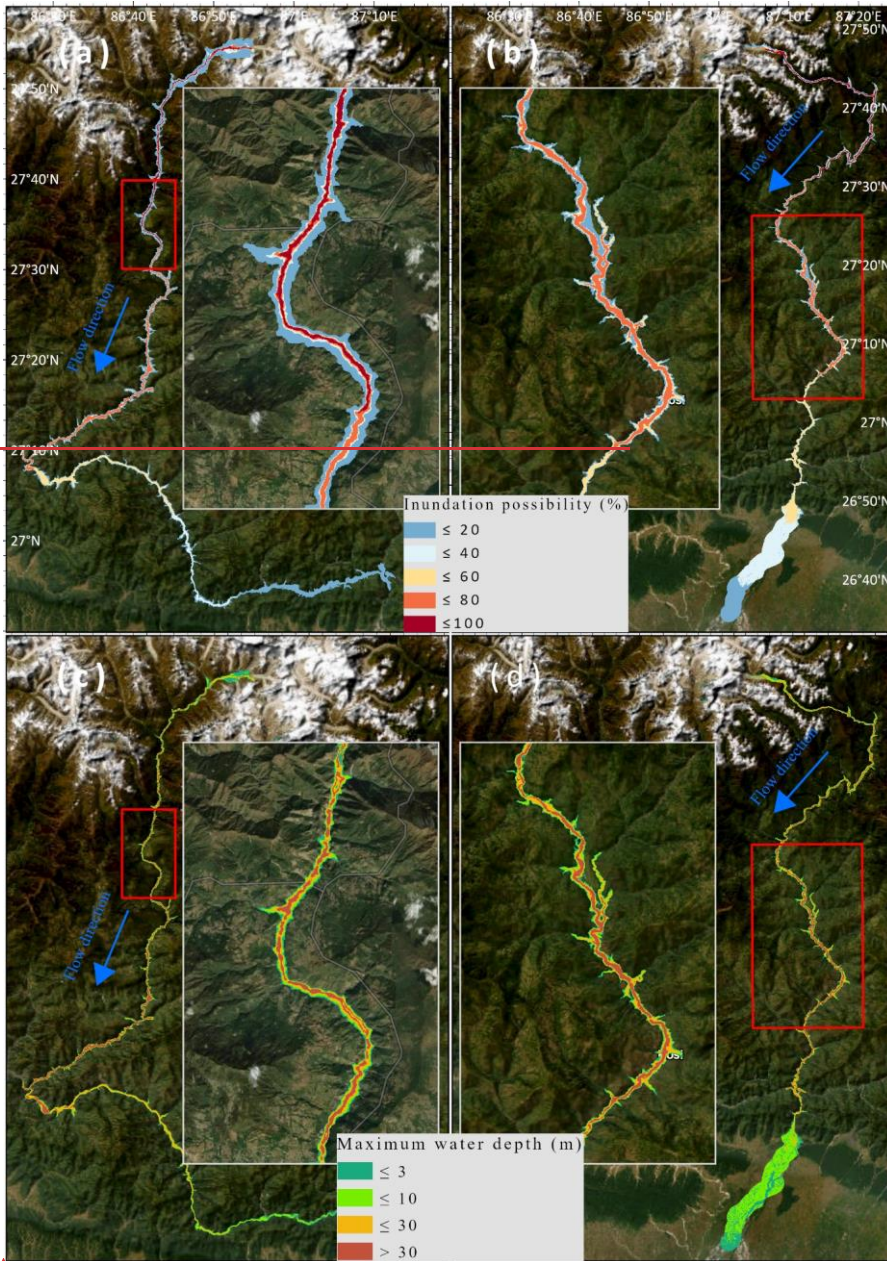
Formatted: Font: (Default) +Body (Times New Roman)

Formatted: Font: (Default) +Body (Times New Roman), (Asian) OpenSans, Font color: Auto

Formatted: Font: (Default) +Body (Times New Roman)

Formatted: Font: (Default) +Body (Times New Roman), (Asian) OpenSans, Font color: Auto

Formatted: Font: (Default) +Body (Times New Roman)

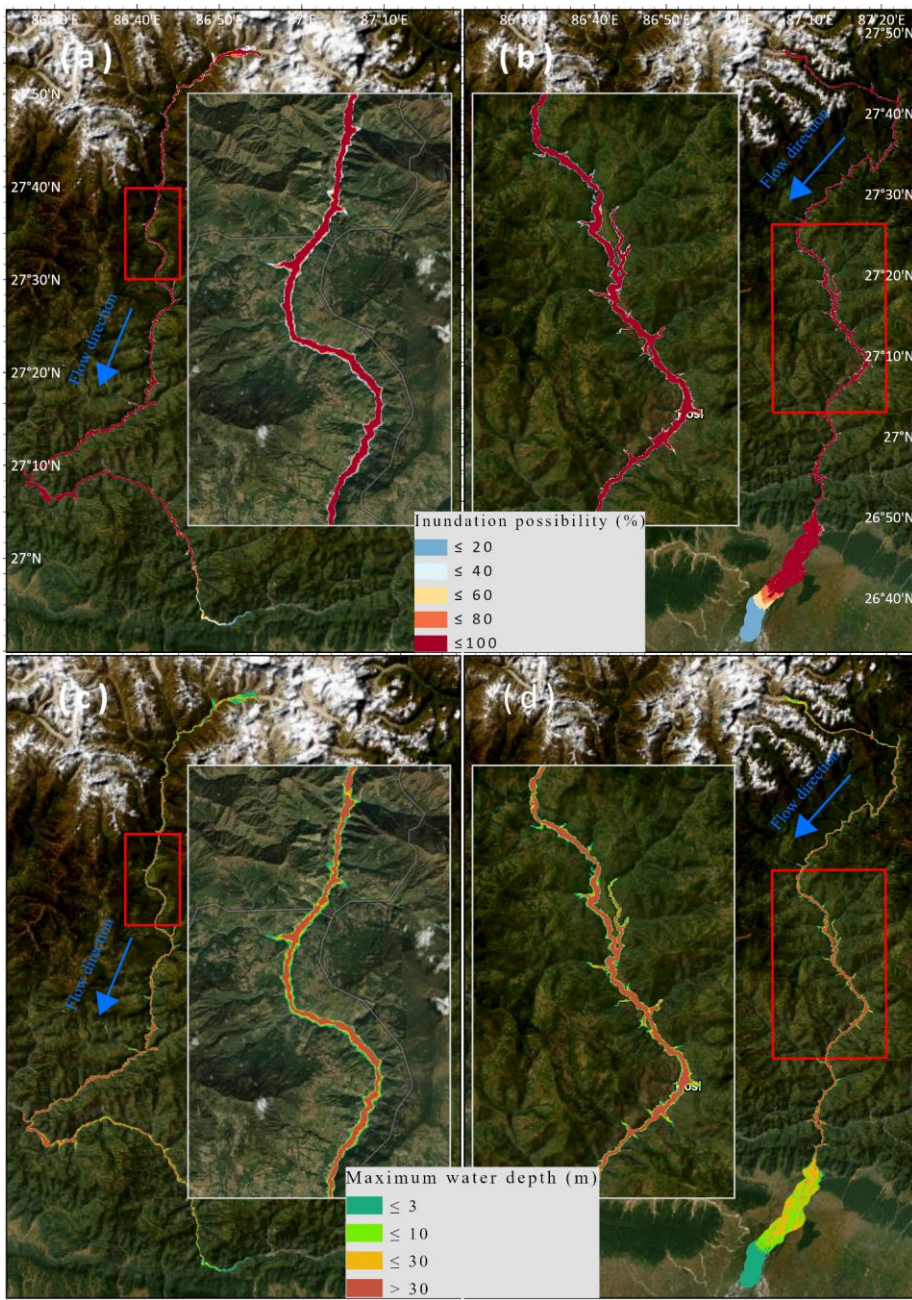


**Formatted:** Font: (Default) +Body (Times New Roman)

**Formatted:** Font: (Default) +Body (Times New Roman)

**Formatted:** Justified, Don't adjust right indent when grid is defined, Don't adjust space between Latin and Asian text, Don't adjust space between Asian text and numbers





415 Fig 5 GLOF inundation probability for (a) Imja Tsho Lake and (b) Lower Barun Lake, and maximum water depth for (c) Imja Tsho Lake and (d) Lower Barun Lake under respective worst situation i.e., all lake water will be released. (The basemaps used were accessed from ArcGIS Online Basemap provided by Esri.)

Formatted: Font: (Default) +Body (Times New Roman)

Formatted: Font: (Default) +Body (Times New Roman)

Formatted: Left

The resulting inundation areas at different levels of inundation probabilities are shown in Fig. 6. The inundation extent resulting from GLOFs originating from the 21 PDGLs ranges from 2.83.6 km<sup>2</sup> to 190.3200.4 km<sup>2</sup>. Notably, the largest glacial lake, Lower Barun (lake number 13), has an inundation area of 18.2172.4 km<sup>2</sup> and 65.3189.5 km<sup>2</sup> for inundation probabilities exceeding 75% and 50%, respectively. Tsho Rolpa Lake (lake number 8), despite having a smaller lake area than Lower Barun, projects inundation areas of 27.6106.9 km<sup>2</sup> and 78.3120.3 km<sup>2</sup> for probabilities exceeding 75% and 50%, respectively. Imja Tsho Lake (lake number 7), similar in size to Tsho Rolpa Lake, anticipates inundation areas of 45.867.2 km<sup>2</sup> and 54.279.6 km<sup>2</sup> for probabilities exceeding 75% and 50%, respectively. It is worth noting that lakes that have not been extensively studied can potentially cause large inundation areas of over 10 km<sup>2</sup> for probabilities exceeding 50%, including Anonymous 7 (86° 55' 41" E, 27° 51' 00" N), Anonymous 8 (86° 55' 01" E, 27° 49' 55" N), Anonymous 11 (86° 51' 29" E, 27° 41' 13" N), Anonymous 12 (85° 37' 51" E, 28° 09' 44" N), Anonymous 1 (87° 44' 59" E, 27° 48' 57" N), and Anonymous 2 (87° 56' 05" E, 27° 47' 26" N). The smallest lake, Anonymous 5 (87° 35' 46" E, 27° 42' 18" N), has an inundation area of 2.5-7 km<sup>2</sup> for probabilities exceeding 50%.

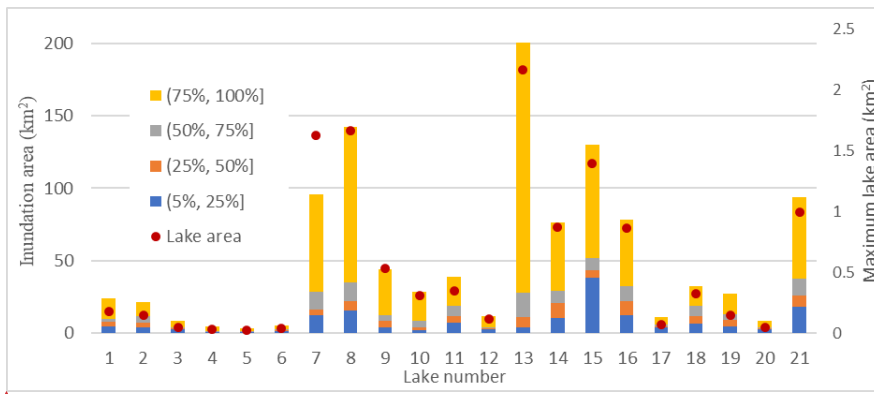
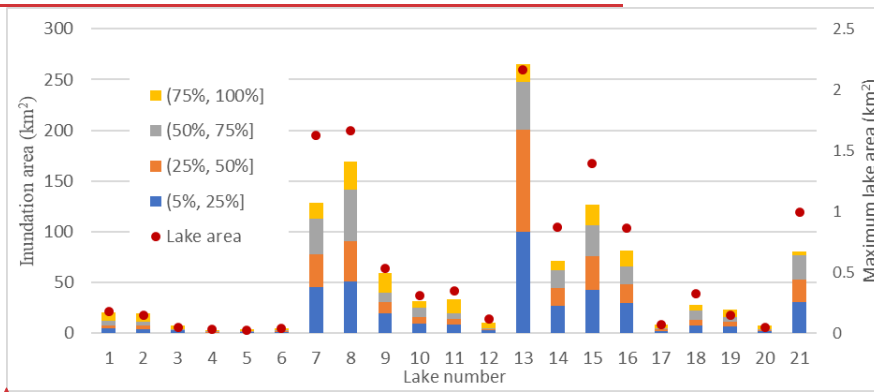


**Fig 6 Inundation area (km<sup>2</sup>) at different levels of inundation probabilities and maximum lake area (km<sup>2</sup>)**

To account for all possible glacial lake outburst scenarios, less severe conditions are also considered, where 25%, 50%, and 75% of the lake water volumemaximum breach depths is/were reached released. In each of these less severe scenarios, 100 cases are randomly selected from a total of 940,000 samples. The outcomes of these scenarios will be compared to the worst-

Formatted: Font: (Default) +Body (Times New Roman), Not Highlight

Formatted: Font: (Default) +Body (Times New Roman)

Formatted: Font: (Default) +Body (Times New Roman), Not Highlight

Formatted: Font: (Default) +Body (Times New Roman)

Formatted: Font: (Default) +Body (Times New Roman)

Formatted: Font: (Default) +Body (Times New Roman)

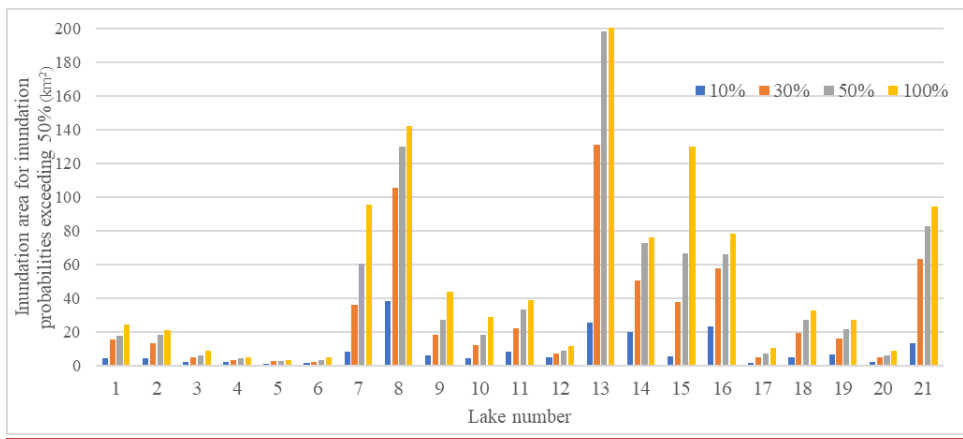
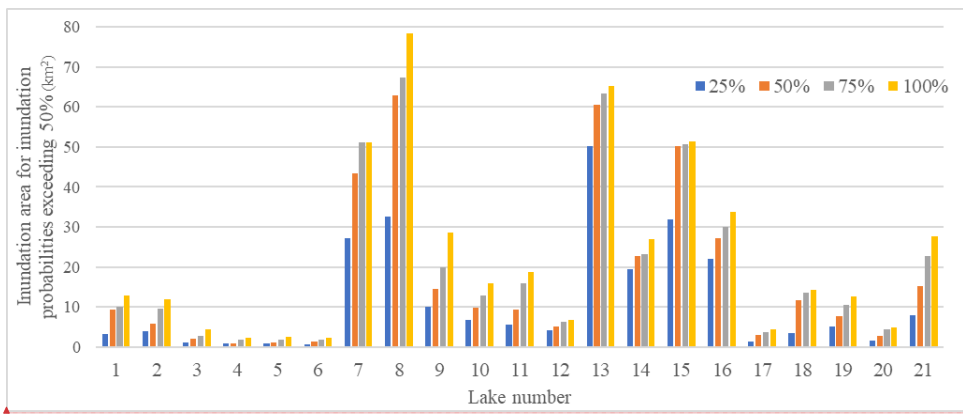
Formatted: Justified, Don't adjust right indent when grid is defined, Don't adjust space between Latin and Asian text, Don't adjust space between Asian text and numbers

Formatted: Font: (Default) +Body (Times New Roman)

Formatted: Font: (Default) +Body (Times New Roman)

Formatted: Left

ease conditions. Fig 7 illustrates the inundation area for inundation probabilities exceeding 50% resulting from GLOFs. In the case of Lower Barun Lake, the release of 25% and 50% of the lake water leads to the inundation of 50.2 km<sup>2</sup> and 60.6 km<sup>2</sup> of downstream areas, respectively. When 100% of the lake water is released, the inundation areas are 1.29 and 1.08 times larger than those under the 25% and 50% lake water release scenarios, respectively. Following Lower Barun Lake, Tsho Rolpa Lake, and Lunding Lake have the potential to cause significant inundation areas. Even with just 25% of the lake water being released, Tsho Rolpa Lake and Imja Tsho Lake can potentially submerge approximately 30 km<sup>2</sup> of areas with inundation probabilities exceeding 50%. To comprehensively evaluate all potential glacial lake outburst scenarios, we also consider less severe conditions, specifically where 10%, 30%, and 50% of the maximum breach depths are reached. In each of these scenarios, 100 representative cases are selected from a total of 940,000 samples using K-means clustering. The outcomes of these less severe scenarios are then compared to the worst-case conditions. Figure 7 illustrates the inundation areas for probabilities exceeding 5% due to GLOFs. For Lower Barun Lake, breaches reaching 10% and 25% of the maximum breach depth result in inundation of 25.5 km<sup>2</sup> and 131.0 km<sup>2</sup> of downstream areas, respectively. When 100% of the maximum breach depth is reached, the inundation areas are 7.87 and 1.53 times larger than those observed in the 10% and 30% maximum breach depth scenarios, respectively. Following Lower Barun Lake, Tsho Rolpa Lake and Lunding Lake also present substantial inundation risks. Even at 10% of the maximum breach depth, Tsho Rolpa Lake has the potential to inundate approximately 40 km<sup>2</sup> of areas with inundation probabilities exceeding 5%.

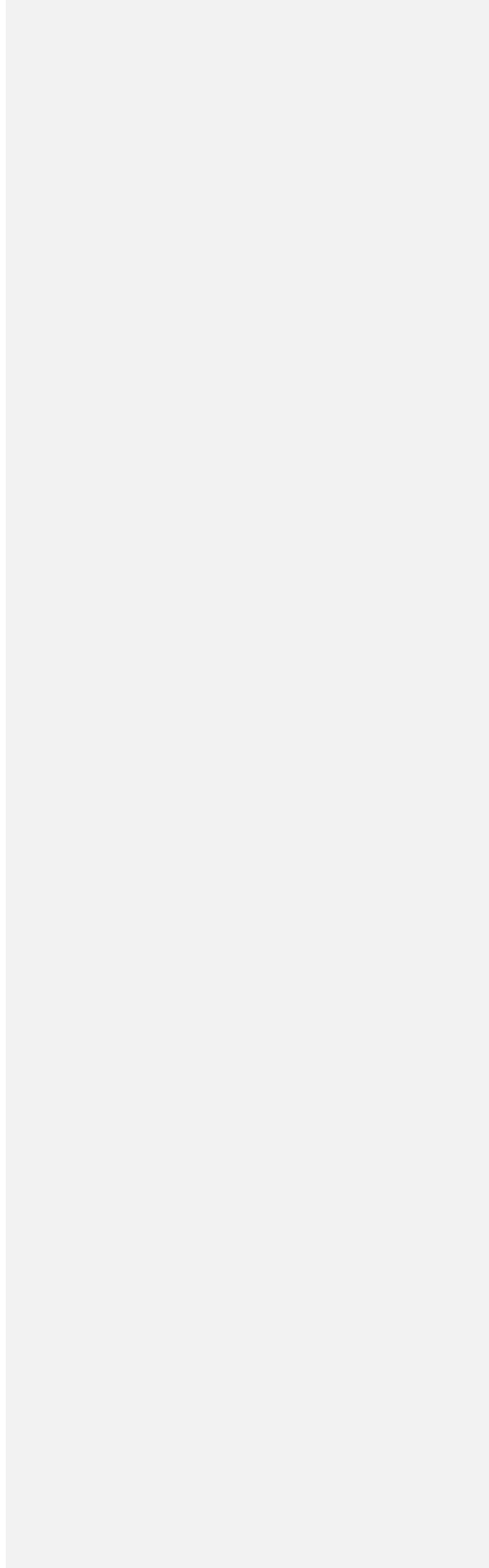


Formatted: Font: (Default) +Body (Times New Roman)

Formatted: Font: (Default) +Body (Times New Roman)

455

Fig 7 Inundation area (km<sup>2</sup>) for inundation probabilities exceeding 50% under 1025%, 3050%, 5075% and 100% of maximum lake-water-volume-dam depth released/reached







### 4.3.2 Exposure assessment

The exposure of objects can be spatially determined by overlaying the predicted flood inundation maps with relevant datasets detailing buildings, roads, and agricultural land (Table 3). Here, we focus on areas with flood probabilities greater than 50%. The number of inundated buildings varies from 011 to 934,388715. Out of the 21 PDGLs, 14 lakes have a number of inundated buildings exceeding 100, while 78 of them inundate at least 1,000 buildings. The three lakes with the highest number of inundated buildings are Tsho Rolpa, Thulagi, Tsho Rolpa, and Lower Barun, each of which could inundate more than 5,000 buildings and cover an area of  $3.7 \times 10^5$  m<sup>2</sup> of building areas. The number of buildings inundated by Tsho Rolpa and Thulagi is 1.7 and 2.5 times that of Lower Barun Lake, respectively. The number of buildings inundated by Tsho Rolpa and Thulagi each is almost twice that of Lower Barun Lake. Overall, these well-studied lakes could impact more buildings than anonymous lakes. These 13 anonymous lakes typically affect fewer than 300 buildings, with the exceptions being Anonymous 17 (87° 44' 59" 86° 55' 41" E, 27° 48' 57" 27° 51' 00" N) and Anonymous 12 (85° 37' 51" E, 28° 09' 44" N), which can influence 665-310 and 1,659-1382 buildings, respectively. Six anonymous lakes including Anonymous 12, 1, 7, 11, 8 and 2 have the potential to impact more than 200 buildings. Further investigation and research are required for the two-six anonymous lakes. Conversely, three lakes, including Anonymous 10 (86° 58' 37" E, 27° 42' 40" N), Anonymous 6 (87° 53' 36" E, 27° 41' 41" N), and Anonymous 9 (87° 05' 42" E, 27° 49' 44" N), pose lower risks, with a number of 40-15 or fewer buildings affected.

Regarding inundated roads, the value ranges from 2-4 to 646721 km. Tsho Rolpa Lake, Thulagi Lake, and Lower Barun Lake still hold the top three positions with the largest lengths of inundated roads, each exceeding 400-350 km. To illustrate, Tsho Rolpa Lake, the top one in this category, inundates a 721-646 km long road. Following closely is Thulagi Lake, which has inundated roads with a length of 419-539 km. Agriculture is a cornerstone of the Nepalese economy, and it is susceptible to the impacts of GLOFs. It is anticipated that twelve lakes have more than 10 km<sup>2</sup> of inundated agricultural land, while three lakes have a negligible impact on agriculture. Lower Barun, Tsho Rolpa, and Thulagi Tsho Rolpa Lake, Lower Barun Lake, and Lunding Lake are still the most perilous lakes concerning the inundation of agricultural lands.

In addition to the high potential for human settlements to be exposed to GLOFs, hydropower projects are increasingly vulnerable to these events. Hydropower development in Nepal has grown rapidly but unevenly. This development trend involves projects moving upstream, bringing hydropower plants closer to glacial lakes. According to the hydropower development data collected in the Hydro Map project (Niti Foundation, n.d.), Nepal has a total of 572 hydropower projects. These projects include 81 that are currently operational, 180 with issued generation licenses, and 311 with issued survey licenses. A total of 49 hydropower plants (as shown in Figure 2, with detailed information provided in the supporting document Table S1) have been identified as being in close proximity to GLOF flow channels, thereby rendering them potentially vulnerable to GLOFs associated with the 21 PDGLs. Among these, 5 plants are currently operational: Madhya Marsyangdi, Marsyangdi, Upper Marsyangdi A, Devighat, Trishuli, and Lower Khare. Additionally, 44 hydropower plants, for which generation or survey licenses have been issued, are also exposed to the risk of GLOFs from these 21 PDGLs. These hydropower plants deserve increased attention in future GLOF risk management due to their significant importance and high vulnerability. In particular, when examining the potential impact of lakes on operational hydropower plants and those holding generation licenses, it is observed that Thulagi Lake and Tsho Rolpa Lake pose a risk of inundating 5 plants (3 operational and 2 licensed) and 3 plants (all licensed), respectively. Moreover, it is noteworthy that lakes Anonymous 12 (85° 37' 51" E, 28° 09' 44" N), Anonymous 1 (87° 44' 59" E, 27° 48' 57" N), and Anonymous 2 (87° 56' 05" E, 27° 47' 26" N) have the potential to inundate 7 plants (2 operational and 6 licensed), 2 plants (both licensed), and 2 plants (both licensed),

Formatted: Font: (Default) +Body (Times New Roman)

Formatted: Automatically adjust right indent when grid is defined, Space After: 0 pt, Adjust space between Latin and Asian text, Adjust space between Asian text and numbers

Formatted: Font: (Default) +Body (Times New Roman)

Formatted: Font: (Default) +Body (Times New Roman)

Formatted: Font: (Default) +Body (Times New Roman)

Formatted: Font: (Default) +Body (Times New Roman)

respectively. Among these, 12 existing hydropower plants (including those in operation and under construction; Table 4) are situated close to GLOF flow channels and are potentially at risk from GLOFs due to 21 PDGLs. The 12 hydropower plants facing such risks are Khimti-I, Upper Tamakoshi, Chatara, Devighat, Trishuli, Marsyangdi, Middle Marsyangdi, Upper Marsyangdi A, Tallo Khare Khola, Arun III, Upper Trishuli-1, and Middle Tamor. Additionally, 38 hydropower plants, for which generation or survey licenses have been issued, are also exposed to the risk of GLOFs from these 21 PDGLs. These hydropower plants deserve increased attention in future GLOF risk management due to their significant importance and high vulnerability. Specifically focusing on certain lakes, Tsho Rolpa, Thulagi, and Lower Barun are responsible for potentially inundating 6 plants (3 existing and 3 with licenses), 6 plants (3 existing and 3 with licenses), and 5 plants (2 existing and 3 with licenses), respectively. Furthermore, Lunding and Imja Tsho can each impact 4 hydropower plants with licenses. Surprisingly, lakes Anonymous 12 (85°-37'-51"-E, 28°-09'-44"-N), Anonymous 1 (87°-44'-59"-E, 27°-48'-57"-N), and Anonymous 2 (87°-56'-05"-E, 27°-47'-26"-N) have the potential to cause the inundation of 10 plants (3 existing and 7 with licenses), 8 plants (1 existing and 7 with licenses), and 6 plants (1 existing and 5 with licenses), respectively.

Table 4 GLOF induced inundation hydropower plants

| Hydropower plant       | State              | Lake name       |
|------------------------|--------------------|-----------------|
| ▲ Khimti I             | Operation          | Tsho Rolpa      |
| ▲ Upper Tamakoshi      | Operation          | Tsho Rolpa      |
| ▲ Chatara              | Operation          | Lower Barun     |
| ▲ Devighat             | Operation          | Anonymous 12    |
| ▲ Trishuli             | Operation          | Anonymous 12    |
| ▲ Marsyangdi           | Operation          | Thulagi         |
| ▲ Middle Marsyangdi    | Operation          | Thulagi         |
| ▲ Upper Marsyangdi A   | Operation          | Thulagi         |
| ▲ Tallo Khare khola    | Under construction | Tsho Rolpa      |
| ▲ Arun III             | Under construction | Lower Barun     |
| ▲ Upper Trishuli-1     | Under construction | Anonymous 12    |
| ▲ Middle Tamor         | Under construction | Anonymous 1 & 2 |
| ▲ Lower Khare          | Generation         | Tsho Rolpa      |
| ▲ Tamakoshi V          | Generation         | Tsho Rolpa      |
| ▲ Langtang Khola Small | Generation         | Anonymous 12    |
| ▲ Upper Trishuli 3A    | Generation         | Anonymous 12    |
| ▲ Upper Trishuli 3B    | Generation         | Anonymous 12    |
| ▲ Marsyangdi Besi      | Generation         | Thulagi         |
| ▲ Upper Tamor          | Generation         | Anonymous 1 & 2 |
| ▲ Upper Tamor A        | Survey             | Anonymous 1     |
| ▲ Dudhkoshi 10         | Survey             | Imja Tsho       |
| ▲ Dudhkoshi 9          | Survey             | Imja Tsho       |
| ▲ Rolwaling Khola      | Survey             | Tsho Rolpa      |
| ▲ Lower Isuwa Khola    | Survey             | Lower Barun     |
| ▲ Lower Bom Khola      | Survey             | Lunding         |
| ▲ Luja Khola           | Survey             | Lunding         |
| ▲ Super Inkhu Khola    | Survey             | Anonymous 11    |
| ▲ Upper Inkhu Khola    | Survey             | Anonymous 11    |
| ▲ Bhotekoshi Khola     | Survey             | Anonymous 12    |

Formatted: Font: (Default) +Body (Times New Roman)

Formatted: Font: (Default) +Body (Times New Roman)

Formatted: Font: (Default) +Body (Times New Roman)

Formatted: Font: (Default) +Body (Times New Roman)

Formatted: Font: (Default) +Body (Times New Roman)

Formatted: Font: (Default) +Body (Times New Roman)

Formatted: Font: (Default) +Body (Times New Roman)

Formatted: Font: (Default) +Body (Times New Roman)

Formatted: Font: (Default) +Body (Times New Roman)

Formatted: Font: (Default) +Body (Times New Roman)

Formatted: Font: (Default) +Body (Times New Roman)

Formatted: Font: (Default) +Body (Times New Roman)

Formatted: Font: (Default) +Body (Times New Roman)

Formatted: Font: (Default) +Body (Times New Roman)

Formatted: Font: (Default) +Body (Times New Roman)

Formatted: Font: (Default) +Body (Times New Roman)

Formatted: Font: (Default) +Body (Times New Roman)

Formatted: Font: (Default) +Body (Times New Roman)

Formatted: Font: (Default) +Body (Times New Roman)

Formatted: Font: (Default) +Body (Times New Roman)

Formatted: Font: (Default) +Body (Times New Roman)

Formatted: Font: (Default) +Body (Times New Roman)

Formatted: Font: (Default) +Body (Times New Roman)

|                          |        |  |
|--------------------------|--------|--|
| Lantang Khola Reservoir  | Survey | Anonymous 12                               |
| Mathillo Langtang        | Survey | Anonymous 12                               |
| Upper Trishuli 1 Cascade | Survey | Anonymous 12                               |
| Rigdi Khola              | Survey | Thulagi                                    |
| Dana Khola               | Survey | Thulagi                                    |
| Tamor Mewa               | Survey | Anonymous 1 & 2                            |
| Tamor Khola-5            | Survey | Anonymous 1 & 2 & 3 & 6                    |
| Ghunsu Tamor             | Survey | Anonymous 1 & 6                            |
| Super Tamor              | Survey | Anonymous 1 & 6                            |
| Upper Tamor HEP          | Survey | Anonymous 1 & 6                            |
| Lower Barun Khola        | Survey | Lower Barun & Anonymous 9                  |
| Upper Barunkhola         | Survey | Lower Barun & Anonymous 9                  |
| Ghunsu Khola             | Survey | Anonymous 2 & 3                            |
| Ghunsu Khola             | Survey | Anonymous 2 & 3                            |
| Chujung Khola            | Survey | Anonymous 4 & 5                            |
| Dudhkoshi-6              | Survey | Imja Tsho, Lumding                         |
| Surke Dudhkoshi          | Survey | Imja Tsho, Lumding                         |
| Hongu Khola I            | Survey | Hongu 1 & 2, Chamlang, Anonymous 7, 8 & 10 |
| Middle Hongu Khola B     | Survey | Hongu 1 & 2, Chamlang, Anonymous 7, 8 & 10 |
| Middle Hongukhola A      | Survey | Hongu 1 & 2, Chamlang, Anonymous 7, 8 & 10 |
| Hongu Khola              | Survey | Hongu 1 & 2, Chamlang, Anonymous 7, 8 & 10 |

Formatted: Font: (Default) +Body (Times New Roman)

Formatted: Font: (Default) +Body (Times New Roman)

Formatted: Font: (Default) +Body (Times New Roman)

Formatted: Font: (Default) +Body (Times New Roman)

Formatted: Font: (Default) +Body (Times New Roman)

Formatted: Font: (Default) +Body (Times New Roman)

Formatted: Font: (Default) +Body (Times New Roman)

Formatted: Font: (Default) +Body (Times New Roman)

Formatted: Font: (Default) +Body (Times New Roman)

Formatted: Font: (Default) +Body (Times New Roman)

Formatted: Font: (Default) +Body (Times New Roman)

Formatted: Font: (Default) +Body (Times New Roman)

Formatted: Font: (Default) +Body (Times New Roman)

Formatted: Font: (Default) +Body (Times New Roman)

Formatted: Font: (Default) +Body (Times New Roman)

Formatted: Font: (Default) +Body (Times New Roman)

Formatted: Font: (Default) +Body (Times New Roman)

Formatted: Font: (Default) +Body (Times New Roman)

Formatted: Font: (Default) +Body (Times New Roman)

Formatted: Font: (Default) +Body (Times New Roman)

Formatted: Font: (Default) +Body (Times New Roman)

Formatted: Font: (Default) +Body (Times New Roman)

Formatted: Font: (Default) +Body (Times New Roman)

Formatted: Font: (Default) +Body (Times New Roman)

Formatted: Font: (Default) +Body (Times New Roman)

Formatted: Font: (Default) +Body (Times New Roman)

#### 4.3.3 Damage Assessment

GLOF damage assessment relies on spatial inundation maps of water depth and depth-damage curves. The inundation maps, depicting water depth, are represented by maximum water depths, for areas with flood probabilities greater than 50%.

515 Following the technical manual of the HAZUS Flood model (FEMA, 2009), damage extents of 1% to 10%, 11% to 50%, and 50% to 100% are defined as slight, moderate, and substantial damage, respectively. Figure 8 uses Lake Anonymous 12 as an example to illustrate the spatial distribution of damage to buildings, roads, and agricultural land caused by GLOFs. Table 3 provides estimates of damage to buildings, roads, and agricultural lands for each lake. In the case of Tsho Rolpa Lake, 7,126 394 buildings are projected to suffer substantial damage from GLOFs. Thulagi Lake and Lower Barun Lake are expected to

520 cause substantial damage to 26,714-520 and 13,338-194 buildings, respectively. Other lakes, such as Imja Tsho Lake and Lumding Lake, are estimated to impact roughly 1,000-160 buildings with substantial damage. Notably, Anonymous 12 (85° 37' 51" E, 28° 09' 44" N) has the potential to affect 1,659-1382 buildings, with 829-964 experiencing moderate impact and 174-375 facing substantial damage. Situated in the Trishuli River Basin, Anonymous 12 not only faces a high hazard level (Rank I) but also high exposure. On the other hand, another anonymous lake (Anonymous 13, at 82° 40' 27" E, 29° 48'

525 09" N) faces a relatively high hazard level (Rank II) but is not projected to cause any substantial damage to buildings due to GLOFs. For PDGLs with a high number of impacted buildings (more than 1,000), except for Anonymous 12, more than 2550% of the impacted buildings are expected to incur substantial damage. In all PDGLs, most affected buildings (over 60%) are predicted to experience moderate or substantial damage. Likewise, over 60% of roads and agricultural lands are anticipated to undergo moderate or substantial damage due to high levels of maximum water depth.

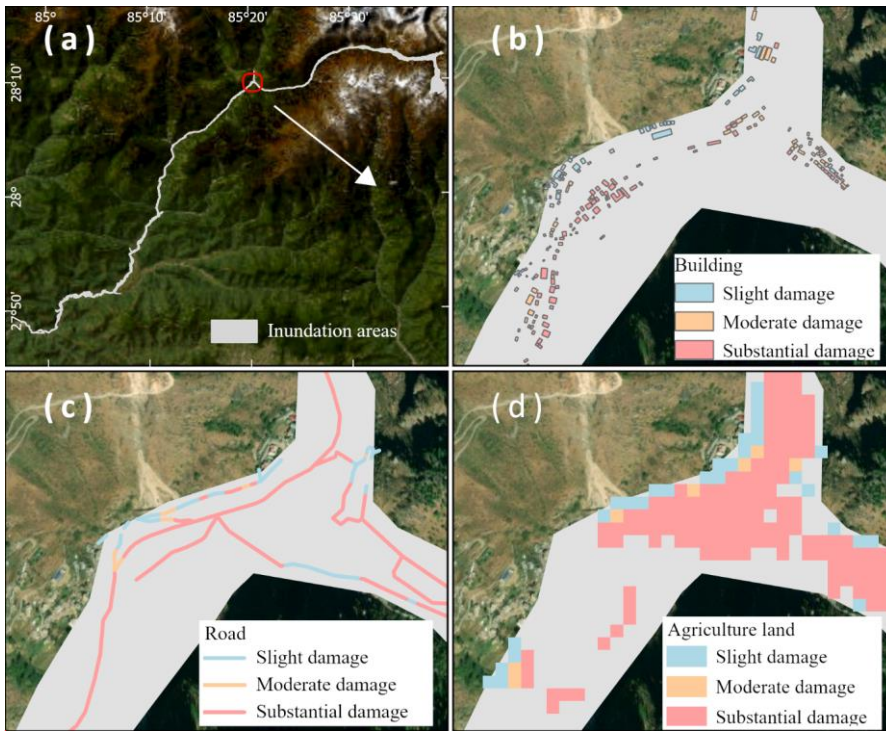


**Fig 8** Damage to buildings, roads, and agricultural land caused by the most serious GLOF due to Lake Anonymous 12

## 5 Discussion

GLOFs can have a significant impact due to the large volume of water stored in glacial lakes, resulting in rapid breaches, high outflow peaks, and high total discharges. While there is a positive correlation between inundation extent and lake area (Fig 6), it's important to note that inundation propagation and extent also depend on dam breach processes as well as the underlying topography and land surface conditions of downstream areas (Worni et al., 2012; Ancey et al., 2019). Particularly, steep and narrow valley gorges can influence flood waves, causing them to rapidly spread over long distances, often accompanied by significant physical processes such as erosion and the transport of ice, sediment, and debris. Among the 21 PDGLs in Nepal, Tsho Rolpa Lake, Thulagi Lake, and Lower Barun Lake are expected to experience the most severe impacts of GLOFs on buildings\_ and roads\_ and\_ while Tsho Rolpa Lake, Lower Barun Lake, and Lunding Lake are anticipated to be the most impacted in terms of GLOFs on agricultural areas. Rounce et al. (2016, 2017) also assessed the downstream impacts of GLOFs from glacial lakes in the Nepal Himalayas. They likewise identified Tsho Rolpa Lake, Lower Barun Lake, and Thulagi Lake as having the most affected buildings, while two anonymous lakes and Thulagi Lake were anticipated to experience the most significant impacts on agricultural areas. However, it's important to note that Rounce et al. (2016, 2017) employed the Monte Carlo least-cost path model (Watson et al., 2015) to estimate the extent of GLOFs for each lake. While the model is computationally efficient and suitable for large-scale applications, it lacks a physical basis and relies solely on the terrain conditions downstream along the river channel, without considering variations in lake release volumes and peak discharges. As a result, flood extents for lakes with differing potential flood volumes may be indistinguishable. Another limitation is that the threshold for the cut-off distance in MC-LCP needs to be artificially set, while the realistic cutoff distance downstream for each lake varies, sometimes extending over 200 km downstream (Richardson & Reynolds, 2000). This study takes a different

Formatted: Font: (Default) +Body (Times New Roman)

Formatted: Font: (Default) +Body (Times New Roman)

Formatted: Left

Formatted: Caption

approach by employing a physics-based hydrodynamic model that predicts not only the inundation extent but also the spatial characteristics of flood features, including inundation probabilities and water depth while considering various outburst scenarios. This information can be used to identify potential exposures and assess the extent of damage to which exposures may be subject.

555 In addition to the growing vulnerability of human settlements in mountainous regions, there is an increasing exposure of  
infrastructure related to energy security and commerce to GLOFs. Therefore, an objective assessment of the risk to  
infrastructure posed by PDGLs is crucial. This study considers hydropower plants, given their critical importance and rapid  
development in Nepal. Nepal is at the heart of a modern resurgence in hydropower development in the Himalayas (Lord et al.,  
2016). The country boasts abundant hydropower resources thanks to its ample river water, steep gradients, and mountainous  
560 terrain. At present, a considerable number of hydropower projects are in the planning and construction stages (46 projects  
exceeding 100 gigawatts) to enhance the country's overall generating capacity. These planned hydropower projects are  
primarily situated along rivers connected to glaciers located in the northern region of Nepal (Shakti et al., 2021). While a few  
existing hydropower plants have experienced direct impacts from recorded GLOFs, such as the Namche hydroelectric power  
plant destroyed by the 1985 Dig Tsho GLOF (Vuichard & Zimmermann, 1987) and the Bhotekoshi hydropower plant affected  
565 by the 2016 GLOF (Cook et al., 2018), GLOFs can be highly destructive and unpredictable, posing a significant threat to  
hydropower facilities. Furthermore, the expansion of hydropower plants into the upstream regions of watersheds substantially  
increases the vulnerability of infrastructure to GLOFs (Nie et al., 2021). Schwanghart et al. (2016) estimated that two-thirds  
of the existing and planned hydropower projects in the Himalayas are located in areas potentially affected by GLOFs, and up  
to one-third of these projects could face GLOF discharges exceeding their local design flood capacities. [In this study, we have  
570 identified 49 existing and planned hydropower projects that could potentially be impacted by GLOFs originating from the 21  
PDGLs; however, we did not assess the specific impacts of GLOFs on these hydropower projects. To our knowledge, there  
are no readily available damage curves that correlate the potential impact on hydropower plants with flood depth and other  
flood characteristics. Furthermore, hydropower plants typically comprise multiple components, including the dam and  
reservoir, powerhouse and auxiliary facilities, among others. The spatial extent of a hydropower plant can vary significantly,  
575 ranging from a few square kilometres to several hundred square kilometres. Accurate assessment would require detailed spatial  
information and mapping of hydropower plants, which is currently lacking. Consequently, this study focuses exclusively on  
identifying whether a hydropower plant is potentially at risk from GLOFs, without engaging in a detailed assessment of the  
specific damages that may be incurred. In this study, we have identified that 50 existing and planned hydropower projects  
could potentially be impacted by GLOFs originating from 21 PDGLs. Still, We strongly urge stakeholders responsible for  
580 planning, designing, constructing, and managing infrastructure to consider these potential GLOF risks. It is crucial to develop  
proactive adaptation measures and adopt sustainable solutions to minimize the negative impacts of GLOFs on infrastructure.](#)

In addition to well-studied PDGLs like Tsho Rolpa Lake, Thulagi Lake, and Lower Barun Lake, some anonymous lakes also  
present a significant risk of GLOFs. For instance, Anonymous 12, [7](#), [1](#), [7](#), [11](#), [8](#), and [2](#) pose high GLOF risks. [Anonymous 12  
\(85°37'51" E, 28°09'44" N\), Anonymous 7 \(86°55'41" E, 27°51'00" N\), Anonymous 1 \(87°44'59" E, 27°48'57" N\), and  
585 Anonymous 11 \(86°51'29" E, 27°41'13" N\) are categorized as Rank I PDGLs, while Anonymous 2 \(87°56'05" N, 27°47'26"  
E; 4950m above sea level\) falls into the Rank III category.](#) GLOFs from any of these [six](#) lakes have the potential to impact  
more than 200 buildings, and GLOFs resulting from Lakes [Anonymous 12](#), [1](#), and [2](#) may submerge existing hydropower  
facilities. Unfortunately, there is limited information available about these anonymous lakes in comparison to well-studied  
PDGLs. To gain a better understanding of their conditions, a comprehensive research strategy is needed, which includes  
590 fieldwork investigations, remote sensing techniques, and [modeling-modelling](#) approaches. This study has leveraged remote  
sensing techniques and [modeling-modelling](#) approaches to preliminarily identify PDGLs with a high level of exposure and  
potential impacts from GLOFs. However, it is imperative to conduct fieldwork investigations, including in situ measurements,

to obtain the essential information required to comprehend the actual state of these anonymous lakes at the local scale. These field investigations will also serve as ground truth to calibrate remote sensing-based data and model outputs. Moreover, considering the challenging nature of fieldwork in glacial lake areas, the cost of expeditions, and the high level of fitness and expertise required by monitoring teams, the preliminary identification of PDGLs with high exposure and potential impacts can offer valuable evidence to support decision-making in the allocation of financial and human resources.

We acknowledge the importance of validating the proposed framework for estimating the impact of GLOFs while recognizing the inherent challenges associated with validation due to the limited availability of historical data. Although Nie et al. (2018), Veh et al. (2019), and Shrestha et al. (2023) have provided valuable inventories of historical GLOFs in the Himalayas, these primarily provide information on the date and location of outbursts, offering limited or no information on the actual impacts resulting from historical GLOFs. Even when impact data is available, it often comprises only generalized descriptions, encompassing metrics like the overall number of casualties, infrastructure damage, and affected villages, lacking specific spatial information. Consequently, obtaining adequate data for validating our proposed impact estimation framework for GLOFs proves challenging. It is noteworthy that our proposed framework employs the fully physically based hydrodynamic model HiPIMS, intricately designed to capture the highly transient and complex hydrodynamic processes induced by events such as dam breaks and flash floods. HiPIMS has been successfully validated for these extreme flow conditions (e.g., Smith and Liang, 2013; Liang et al., 2016). The adoption of this model enhances our confidence in simulating the spatial-temporal processes of GLOF inundation, ultimately contributing to improved hazard evaluation results. Furthermore, we employ Bayesian approaches to derive plausible value ranges for lake volumes and peak discharges. These approaches facilitate the creation of multiple GLOF scenarios for each glacial lake, ensuring comprehensive coverage of all potential glacial lake outburst scenarios. The incorporation of Bayesian methods allows us to account for uncertainties, thereby enhancing the robustness of our impact evaluation for potentially devastating GLOFs.

## 6 Conclusion

Exposure and damage estimations are integral components of GLOF risk assessment. Having sufficient information about the potential impacts of GLOFs originating from PDGLs is essential to facilitate GLOF risk management. In this study, we harnessed multi-temporal satellite imagery, Bayesian regression models that establish relationships between lake areas and depths, as well as between flood volume and peak discharge, and a high-performance hydrodynamic flood model to support GLOF exposure and damage assessments for multiple lakes. We applied this assessment framework to 21 PDGLs identified in the Nepal Himalaya, and the key findings of this study are summarized as follows:

- Utilizing multi-temporal imagery capturing different hydrological conditions of glacial lakes enables the derivation of the full or maximum glacial lake boundaries for potential risk assessment.
- The Bayesian regression model, which establishes relationships between lake areas and depths, as well as between flood volume and peak discharge, can produce predictive posterior distributions for lake depths and peak discharges for each lake. These distributions offer a plausible range of values for lake volumes and peak discharges for each PDGL, facilitating subsequent objective flood ~~modeling-modelling~~ and impact analysis.
- The hydrodynamic model (HiPIMS), supported by parallelized high-performance GPU computation, is capable of predicting the resulting GLOFs in terms of temporally and spatially varying flood frequency and water depths to reflect the highly transient flood dynamics under various scenarios for multiple glacial lakes on a large scale.
- Among the 21 PDGLs identified in the Nepal Himalayas, Tsho Rolpa Lake, Thulagi Lake, and Lower Barun Lake are poised to bear the most severe impacts of GLOFs on buildings, ~~and roads. Meanwhile, Tsho Rolpa Lake, Lower Barun Lake, and Lumding Lake will encounter the most significant GLOF impacts on, and~~ agricultural areas. ~~Four-Six~~



635

anonymous lakes, specifically Anonymous 12 (85°37'51" E, 28°09'44" N), Anonymous 1 (87°44'59" E, 27°48'57" N), Anonymous 7 (86°55'41" E, 27°51'00" N), ~~Anonymous 1 (87°44'59" E, 27°48'57" N)~~, Anonymous 11 (86°51'29" E, 27°41'13" N), Anonymous 8 (86°55'01" E, 27°49'55" N), and Anonymous 2 (87°56'05" N, 27°47'26" E), have the potential to impact more than 200 buildings. The GLOFs from these 21 PDGLs can also impact the 5±2 existing hydropower plants and the 3844 hydropower projects that have been granted generation or survey licenses.

640

Notably, Anonymous 12, ~~1, and 2~~ may even submerge existing hydropower facilities. ~~The GLOFs from these 21 PDGLs can also impact the 12 existing hydropower plants and the 38 hydropower projects that have been granted generation or survey licenses.~~

**Appendix:** List of abbreviations used in this study.

|               |   |
|---------------|---|
| CI            | confidence interval                                       |
| <u>DEM</u>    | <u>digital elevation model</u>                            |
| <u>EVI</u>    | Enhanced Vegetation Index                                 |
| <u>GIS</u>    | Geographic Information System                             |
| <u>GLOFs</u>  | Glacial Lake Outburst Floods                              |
| <u>GPU</u>    | Graphics processing unit                                  |
| <u>HDI</u>    | highest density interval                                  |
| <u>HiPIMS</u> | High-Performance Integrated Hydrodynamic Modelling System |
| <u>MNDWI</u>  | Modified Normalized Difference Water Index                |
| <u>NIR</u>    | Near Infrared   |
| <u>NDMI</u>   | Normalized Difference Moisture Index                      |
| <u>NDVI</u>   | Normalized Difference Vegetation Index                    |
| <u>NDWI</u>   | Normalized Difference Water Index                         |
| <u>OSM</u>    | OpenStreetMap   |
| <u>PDGL</u>   | potentially dangerous glacial lake                        |
| <u>SRTM</u>   | Shuttle Radar Topography Mission                          |
| <u>TOA</u>    | Top-Of-Atmosphere   |

**References**

Ancey, C., Bardou, E., Funk, M., Huss, M., Werder, M. A., & Trehwela, T. (2019). Hydraulic reconstruction of the 1818 Giétro glacial lake outburst flood. *Water Resources Research*, 55(11), 8840-8863.

Arcement, G. J., & Schneider, V. R. (1989). Guide for selecting Manning's roughness coefficients for natural channels and flood plains. Washington, DC: US Government Printing Office.

Bajracharya, S. R., Maharjan, S. B., Shrestha, F., Sherpa, T. C., Wagle, N., & Shrestha, A. B. (2020). Inventory of glacial lakes and identification of potentially dangerous glacial lakes in the Koshi, Gandaki, and Karnali River Basins of Nepal, the Tibet Autonomous Region of China. International Centre for Integrated Mountain Development GPO Box, 3226.

Barnes, H. H. (1967). Roughness characteristics of natural channels. US Government Printing Office.

Formatted: Font: (Default) +Body (Times New Roman), Font color: Auto

Formatted: Font: (Default) +Body (Times New Roman)

Formatted: Font: (Default) +Body (Times New Roman), Font color: Auto

Formatted: Font: (Default) +Body (Times New Roman)

Formatted: Font: (Default) +Body (Times New Roman)

Formatted: Font: (Default) +Body (Times New Roman)

Formatted: Font: (Default) +Body (Times New Roman)

Formatted: Font: (Default) +Body (Times New Roman)

Formatted: Font: (Default) +Body (Times New Roman)

Formatted: Font: (Default) +Body (Times New Roman)

Formatted: Font: (Default) +Body (Times New Roman)

Formatted: Font: (Default) +Body (Times New Roman)

Formatted: Font: (Default) +Body (Times New Roman)

Formatted: Font: (Default) +Body (Times New Roman)

Formatted: Font: (Default) +Body (Times New Roman)

Formatted: Font: (Default) +Body (Times New Roman)

Formatted: Font: (Default) +Body (Times New Roman)

Formatted: Font: (Default) +Body (Times New Roman)

Formatted: Font: (Default) +Body (Times New Roman)

Formatted: Font: (Default) +Body (Times New Roman)

Formatted: Font: (Default) +Body (Times New Roman)

Formatted: Font: (Default) +Body (Times New Roman)

Formatted: Font: (Default) +Body (Times New Roman)

Formatted: Font: (Default) +Body (Times New Roman)

Formatted: Font: (Default) +Body (Times New Roman)

- Bishop, C. M., & Tipping, M. E. (2003). Bayesian regression and classification. *Nato Science Series sub Series III Computer And Systems Sciences*, 190, 267-288.
- Breiman, L. (2001). Random forests. *Machine learning*, 45(1), 5-32.
- 655 Budhathoki, K. P., Bajracharya, O. R., & Pokharel, B. K. (2010). Assessment of Imja Glacier Lake outburst flood (GLOF) risk in Dudh Koshi River Basin using remote sensing techniques. *Journal of Hydrology and Meteorology*, 7(1), 75-91.
- Chen, H., Liang, Q., Liang, Z., Liu, Y., & Ren, T. (2020). Extraction of connected river networks from multi-temporal remote sensing imagery using a path tracking technique. *Remote Sensing of Environment*, 246, 111868.
- Chen, H., Zhao, J., Liang, Q., Maharjan, S. B., & Joshi, S. P. (2022). Assessing the potential impact of glacial lake outburst  
660 floods on individual objects using a high-performance hydrodynamic model and open-source data. *Science of The Total Environment*, 806, 151289.
- Chow, V.T., (1959). *Open-channel Hydraulics*. Book Co., New York, McGraw-Hill, p.680.
- Cook, K. L., Andermann, C., Gimbert, F., Adhikari, B. R., & Hovius, N. (2018). Glacial lake outburst floods as drivers of fluvial erosion in the Himalaya. *Science*, 362(6410), 53-57.
- 665 Cook, S. J., & Quincey, D. J. (2015). Estimating the volume of Alpine glacial lakes. *Earth Surface Dynamics*, 3(4), 559-575.
- Dubey, S., & Goyal, M. K. (2020). Glacial lake outburst flood hazard, downstream impact, and risk over the Indian Himalayas. *Water Resources Research*, 56(4), e2019WR026533.
- Ellison, A. M. (2004). Bayesian inference in ecology. *Ecology letters*, 7(6), 509-520.
- Farr, T. G., Rosen, P. A., Caro, E., Crippen, R., Duren, R., Hensley, S., ... & Alsdorf, D. (2007). The shuttle radar  
670 topography mission. *Reviews of geophysics*, 45(2).
- FEMA. (2009). Multi-hazard loss estimation methodology: Flood model. HAZUS-MH MR3 technical manual. P220.
- Gao, B. C. (1996). NDWI—A normalized difference water index for remote sensing of vegetation liquid water from space. *Remote sensing of environment*, 58(3), 257-266.
- Ghimire, M. (2004). Review of studies on glacier lake outburst floods and associated vulnerability in the  
675 Himalayas. *Himalayan Review*, 49-64.
- Granshaw, F. D., & Fountain, A. G. (2006). Glacier change (1958–1998) in the north Cascades national park complex, Washington, USA. *Journal of Glaciology*, 52(177), 251-256.
- Haritashya, U. K., Kargel, J. S., Shugar, D. H., Leonard, G. J., Strattman, K., Watson, C. S., ... & Regmi, D. (2018). Evolution and controls of large glacial lakes in the Nepal Himalaya. *Remote Sensing*, 10(5), 798.
- 680 Huete, A., Didan, K., Miura, T., Rodriguez, E. P., Gao, X., & Ferreira, L. G. (2002). Overview of the radiometric and biophysical performance of the MODIS vegetation indices. *Remote sensing of environment*, 83(1-2), 195-213.
- Huggel, C., Kääb, A., Haerberli, W., Teyssie, P., & Paul, F. (2002). Remote sensing based assessment of hazards from glacier lake outbursts: a case study in the Swiss Alps. *Canadian Geotechnical Journal*, 39(2), 316-330.
- Huizinga, J., De Moel, H., & Szwedczyk, W. (2017). Global flood depth-damage functions: Methodology and the database  
685 with guidelines (No. JRC105688). Joint Research Centre (Seville site).
- Kapitsa, V., Shahgedanova, M., Machguth, H., Severskiy, I., & Medeu, A. (2017). Assessment of evolution and risks of glacier lake outbursts in the Djungarskiy Alatau, Central Asia, using Landsat imagery and glacier bed topography modelling. *Natural Hazards and Earth System Sciences*, 17(10), 1837-1856.
- Khadka, N., Zhang, G., & Chen, W. (2019). The state of six dangerous glacial lakes in the Nepalese Himalaya. TAO:  
690 Terrestrial, Atmospheric and Oceanic Sciences, 30(1), 6.
- Krause, L., Mal, S., Karki, R., & Schickhoff, U. (2019). Recession of Trakarding glacier and expansion of Tsho Rolpa lake in Nepal Himalaya based on satellite data. *Himalayan Geology*, 40(2), 103-114.
- Lala, J. M., Rounce, D. R., & McKinney, D. C. (2017). Modeling the glacial lake outburst flood process chain in the Nepal Himalaya: reassessing Imja Tsho's hazard. *Hydrology and Earth System Sciences*, 22, 3721–3737



- 695 Lamsal, D., Sawagaki, T., Watanabe, T., & Byers, A. C. (2016). Assessment of glacial lake development and prospects of  
 outburst susceptibility: Chamlang South Glacier, eastern Nepal Himalaya. *Geomatics, Natural Hazards and Risk*, 7(1), 403-  
 423.
- Land cover of Nepal 2010 <http://rds.icimod.org/Home/DataDetail?metadataId=9224> (2020) Accessed 2020-04-26
- Lord, A. (2016). Citizens of a hydropower nation: Territory and agency at the frontiers of hydropower development in  
 700 Nepal. *Economic Anthropology*, 3(1), 145-160.
- Liang, Q., Chen, K. C., Jingming, H. O. U., Xiong, Y., Gang, W., & Qiang, J. (2016). Hydrodynamic modelling of flow  
 impact on structures under extreme flow conditions. *Journal of Hydrodynamics*, Ser. B, 28(2), 267-274.
- McFeeters, S. K. (1996). The use of the Normalized Difference Water Index (NDWI) in the delineation of open water  
 features. *International journal of remote sensing*, 17(7), 1425-1432.
- 705 Mool, P. K., Maskey, P. R., Koirala, A., Joshi, S. P., Lizong, W., Shrestha, A. B., ... & Shrestha, R. B. (2011). Glacial lakes  
 and glacial lake outburst floods in Nepal. [https://policycommons.net/artifacts/1516291/glacial-lakes-and-glacial-lake-  
 outburst-floods-in-nepal/2192662/](https://policycommons.net/artifacts/1516291/glacial-lakes-and-glacial-lake-outburst-floods-in-nepal/2192662/). Accessed 2022-04-26
- Morris, M. W., Hassan, M. A. A. M., & Vaskinn, K. A. (2007). Breach formation: Field test and laboratory experiments.  
*Journal of Hydraulic Research*, 45(sup1), 9-17.
- 710 Muñoz, R., Huggel, C., Frey, H., Cochachin, A., & Haeblerli, W. (2020). Glacial lake depth and volume estimation based on  
 a large bathymetric dataset from the Cordillera Blanca, Peru. *Earth surface processes and landforms*, 45(7), 1510-1527.
- Nepal Hydropower portal. (2019) Available at: <https://hydro.naxa.com.np/core/about> Accessed 22 August 2023.
- Nie, Y., Liu, Q., Wang, J., Zhang, Y., Sheng, Y., & Liu, S. (2018). An inventory of historical glacial lake outburst floods in  
 the Himalayas based on remote sensing observations and geomorphological analysis. *Geomorphology*, 308, 91-106. Nie, Y.,  
 715 Pritchard, H. D., Liu, Q., Hennig, T., Wang, W., Wang, X., ... & Chen, X. (2021). Glacial change and hydrological  
 implications in the Himalaya and Karakoram. *Nature reviews earth & environment*, 2(2), 91-106.
- Nie, Y., Sheng, Y., Liu, Q., Liu, L., Liu, S., Zhang, Y., & Song, C. (2017). A regional-scale assessment of Himalayan glacial  
 lake changes using satellite observations from 1990 to 2015. *Remote Sensing of Environment*, 189, 1-13.
- OpenStreetMap data for Nepal <http://download.geofabrik.de/asia/nepal.html> (2015) Accessed 2022-04-26
- 720 Rana, B., Shrestha, A. B., Reynolds, J. M., Aryal, R., Pokhrel, A. P., & Budhathoki, K. P. (2000). Hazard assessment of the  
 Tsho Rolpa Glacier Lake and ongoing remediation measures. *Journal of Nepal Geological Society*, 22, 563.
- Richardson, S. D., & Reynolds, J. M. (2000). An overview of glacial hazards in the Himalayas. *Quaternary  
 International*, 65, 31-47.
- Rinzin, S., Zhang, G., Sattar, A., Wangchuk, S., Allen, S. K., Dunning, S., & Peng, M. (2023). GLOF hazard, exposure,  
 725 vulnerability, and risk assessment of potentially dangerous glacial lakes in the Bhutan Himalaya. *Journal of Hydrology*, 619,  
 129311.
- Rodriguez-Galiano, V. F., Ghimire, B., Rogan, J., Chica-Olmo, M., & Rigol-Sanchez, J. P. (2012). An assessment of the  
 effectiveness of a random forest classifier for land-cover classification. *ISPRS journal of photogrammetry and remote  
 sensing*, 67, 93-104.
- 730 Rounce, D. R., McKinney, D. C., Lala, J. M., Byers, A. C., & Watson, C. S. (2016). A new remote hazard and risk  
 assessment framework for glacial lakes in the Nepal Himalaya. *Hydrology and Earth System Sciences*, 20(9), 3455-3475.
- Rounce, D. R., Watson, C. S., & McKinney, D. C. (2017). Identification of hazard and risk for glacial lakes in the Nepal  
 Himalaya using satellite imagery from 2000–2015. *Remote Sensing*, 9(7), 654.
- Sattar, A., Goswami, A., & Kulkarni, A. V. (2019). Hydrodynamic moraine-breach modeling and outburst flood routing-A  
 735 hazard assessment of the South Lhonak lake, Sikkim. *Science of the total environment*, 668, 362-378.
- Sattar, A., Haritashya, U. K., Kargel, J. S., Leonard, G. J., Shugar, D. H., & Chase, D. V. (2021). Modeling lake outburst and  
 downstream hazard assessment of the Lower Barun Glacial Lake, Nepal Himalaya. *Journal of Hydrology*, 598, 126208.

- Scawthorn, C., Flores, P., Blais, N., Seligson, H., Tate, E., Chang, S., ... & Lawrence, M. (2006). HAZUS-MH flood loss estimation methodology. II. Damage and loss assessment. *Natural Hazards Review*, 7(2), 72-81.
- 740 Schaffer-Smith, D., Swenson, J. J., Barbaree, B., & Reiter, M. E. (2017). Three decades of Landsat-derived spring surface water dynamics in an agricultural wetland mosaic; Implications for migratory shorebirds. *Remote Sensing of Environment*, 193, 180-192.
- Schwanghart, W., Wormi, R., Huggel, C., Stoffel, M., & Korup, O. (2016). Uncertainty in the Himalayan energy–water nexus: Estimating regional exposure to glacial lake outburst floods. *Environmental Research Letters*, 11(7), 074005.
- 745 Shakti, P. C., Pun, I., Talchabhadel, R., & Kshetri, D. (2021). The Role of Glaciers in Hydropower Production in Nepal. *Journal of Asian Energy Studies*, 5(1), 1-13.
- Shrestha, B. B., & Nakagawa, H. (2014). Assessment of potential outburst floods from the Tsho Rolpa glacial lake in Nepal. *Natural Hazards*, 71(1), 913-936.
- Shrestha, F., Steiner, J. F., Shrestha, R., Dhungel, Y., Joshi, S. P., Inglis, S., ... & Zhang, T. (2023). A comprehensive and version-controlled database of glacial lake outburst floods in High Mountain Asia. *Earth System Science Data*, 15(9), 3941-3961.
- 750 Shugar, D. H., Burr, A., Haritashya, U. K., Kargel, J. S., Watson, C. S., Kennedy, M. C., ... & Stratman, K. (2020). Rapid worldwide growth of glacial lakes since 1990. *Nature Climate Change*, 10(10), 939-945.
- Somos-Valenzuela, M. A., McKinney, D. C., Byers, A. C., Rounce, D. R., Portocarrero, C., & Lamsal, D. (2015). Assessing downstream flood impacts due to a potential GLOF from Imja Tsho in Nepal. *Hydrology and Earth System Sciences*, 19(3), 1401-1412.
- 755 Smith, L. S., & Liang, Q. (2013). Towards a generalised GPU/CPU shallow-flow modelling tool. *Computers & Fluids*, 88, 334-343.
- Somos-Valenzuela, M. A., McKinney, D. C., Rounce, D. R., & Byers, A. C. (2014). Changes in Imja Tsho in the Mount Everest region of Nepal. *The Cryosphere*, 8(5), 1661-1671.
- 760 Tucker, C. J. (1979). Red and photographic infrared linear combinations for monitoring vegetation. *Remote sensing of Environment*, 8(2), 127-150.
- Tulbure, M. G., Broich, M., Stehman, S. V., & Kommareddy, A. (2016). Surface water extent dynamics from three decades of seasonally continuous Landsat time series at subcontinental scale in a semi-arid region. *Remote Sensing of Environment*, 178, 142-157.
- 765 Veh, G., Korup, O., von Specht, S., Roessner, S., & Walz, A. (2019). Unchanged frequency of moraine-dammed glacial lake outburst floods in the Himalaya. *Nature Climate Change*, 9(5), 379-383.
- Veh, G., Korup, O., & Walz, A. (2020). Hazard from Himalayan glacier lake outburst floods. *Proceedings of the National Academy of Sciences*, 117(2), 907-912.
- 770 Vuichard, D., & Zimmermann, M. (1987). The 1985 catastrophic drainage of a moraine-dammed lake, Khumbu Himal, Nepal: cause and consequences. *Mountain Research and Development*, 91-110.
- Walder, J. S., Iverson, R. M., Godt, J. W., Logan, M., & Solovitz, S. A. (2015). Controls on the breach geometry and flood hydrograph during overtopping of noncohesive earthen dams. *Water Resources Research*, 51(8), 6701-6724.
- 775 Walder, J. S., & O'Connor, J. E. (1997). Methods for predicting peak discharge of floods caused by failure of natural and constructed earthen dams. *Water Resources Research*, 33(10), 2337-2348.
- Watson, C. S., Carrivick, J., & Quincey, D. (2015). An improved method to represent DEM uncertainty in glacial lake outburst flood propagation using stochastic simulations. *Journal of Hydrology*, 529, 1373-1389.
- Worni, R., Huggel, C., & Stoffel, M. (2013). Glacial lakes in the Indian Himalayas—From an area-wide glacial lake inventory to on-site and modeling based risk assessment of critical glacial lakes. *Science of the Total Environment*, 468, S71-S84.
- 780 S84.

Formatted: Font: (Default) +Body (Times New Roman)

Worni, R., Stoffel, M., Huggel, C., Volz, C., Castellor, A., & Luckman, B. (2012). Analysis and dynamic modeling of a moraine failure and glacier lake outburst flood at Ventisquero Negro, Patagonian Andes (Argentina). *Journal of Hydrology*, 444, 134-145.

785 Xu, H. (2006). Modification of normalised difference water index (NDWI) to enhance open water features in remotely sensed imagery. *International journal of remote sensing*, 27(14), 3025-3033.

Yang, M., Cai, Q., Li, Z., & Yang, J. (2023). Uncertainty analysis on flood routing of embankment dam breach due to overtopping failure. *Scientific Reports*, 13(1), 20151.

Yang, Y., Cao, S. Y., Yang, K. J., & Li, W. P. (2015). Experimental study of breach process of landslide dams by overtopping and its initiation mechanisms. *Journal of Hydrodynamics*, 27(6), 872-883.

790 Yu, X., Hyypää, J., Vastaranta, M., Holopainen, M., & Viitala, R. (2011). Predicting individual tree attributes from airborne laser point clouds based on the random forests technique. *ISPRS Journal of Photogrammetry and remote sensing*, 66(1), 28-37.

Zhang, G., Yao, T., Xie, H., Wang, W., & Yang, W. (2015). An inventory of glacial lakes in the Third Pole region and their changes in response to global warming. *Global and Planetary Change*, 131, 148-157.

795 Zhao, J., & Liang, Q. (2022). Novel variable reconstruction and friction term discretisation schemes for hydrodynamic modelling of overland flow and surface water flooding. *Advances in Water Resources*, 163, 104187.

Zhang, T., Wang, W., & An, B. (2023a). A conceptual model for glacial lake bathymetric distribution. *The Cryosphere Discussions*, 2023, 1-35.

800 Zhang, T., Wang, W., An, B., & Wei, L. (2023b). Enhanced glacial lake activity threatens numerous communities and infrastructure in the Third Pole. *Nature Communications*, 14(1), 8250.

Zheng, G., Allen, S. K., Bao, A., Ballesteros-Cánovas, J. A., Huss, M., Zhang, G., ... & Stoffel, M. (2021). Increasing risk of glacial lake outburst floods from future Third Pole deglaciation. *Nature Climate Change*, 11(5), 411-417.

#### **Data availability**

805 The DEM used in this work is the SRTM DEM. Land use types are extracted from the Landsat TM imagery from the year 2010, which can be accessed at <http://rds.icimod.org/Home/DataDetail?metadataId=9224>. The OpenStreetMap (OSM) data can be accessed via the link <http://download.geofabrik.de/asia/nepal.html>. Hydropower plant data are obtained from the Hydro Map project through the link <https://hydro.naxa.com.np/core/about>.

#### **Code availability**

The flood model can be accessed through the link <https://github.com/HEMLab/HiPIMS-CUDA>.

#### **810 Author contribution**

HC was responsible for developing the methodology, conducting analysis, and drafting the paper. QL handled funding acquisition, research design, and reviewing and refining the draft. JZ developed the flood model codes, and SM provided a review of the draft.

#### **Competing interests**

815 The contact author has declared that none of the authors has any competing interests.

Formatted: Font: (Default) +Body (Times New Roman)

Formatted: Font: (Default) +Body (Times New Roman)

Formatted: Font: (Default) +Body (Times New Roman)

Formatted: Font: (Default) +Body (Times New Roman)

Formatted: Font: (Default) +Body (Times New Roman)

Formatted: Font: (Default) +Body (Times New Roman)

Formatted: Font: (Default) +Body (Times New Roman)

Formatted: Font: (Default) +Body (Times New Roman)

Formatted: Font: (Default) +Body (Times New Roman)

Formatted: Font: (Default) +Body (Times New Roman)

Formatted: Font: (Default) +Body (Times New Roman)

**Acknowledgments**

This work is supported by the WeACT project (NE/S005919/1) funded by the UK Natural Environment Research Council (NERC) through the SHEAR programme.

Formatted: Font: (Default) +Body (Times New Roman)

Formatted: Font: (Default) +Body (Times New Roman)

Formatted: Font: (Default) +Body (Times New Roman)